FIGURE 1: Widespread preferential glial transduction of mouse brains after intracardiac injections of tyrosine-mutant AAV9/3 vectors containing a ubiquitous promoter. The tyrosine-mutant AAV9/3 vector expressed green fluorescent protein (GFP) under control of the cytomegalovirus immediate-early enhancer and chicken β-actin (CAG) promoter. ((a)–(d)) Representative images of coronal sections stained with an anti-GFP antibody following virus administration. Section locations relative to the Bregma: (a) +1.34 mm; (b) +0.14 mm; (c) –1.70 mm; and (d) –6.24 mm. ((e), (f)) Merged images showing results of double immunostaining experiments. Most transduced cells showed glial morphologies and were immunoreactive for glial fibrillary acidic protein (GFAP) but not NeuN. (e) GFP (green), NeuN (red); and (f) GFP (green), GFAP (red). Analysis of GFP expression in peripheral organs revealed robust transduction of the heart, liver, and kidney (g–i). Scale bars: ((a)–(d)) 2 mm; ((e), (f), insets of (g)–(i)) 30 μm; ((g)–(i)) 1 mm.

3.2. Neuronal Transduction Was Achieved with Specific Promoters. We next made AAV9/3 vectors that expressed GFP under control of the neuron-specific synapsin I promoter and were encapsulated with double tyrosine-mutant capsid proteins (yfAAV9/3-SynI-GFP). Six weeks after intracardiac infusions of the vectors into adult mice, robust transductions were observed throughout the brains (Figures 2(a)–2(d)). Double immunofluorescence stainings demonstrated that nearly all GFP-IR cells expressed the neuronal marker NeuN (NeuN-IR) (Figure 2(e)). When the yfAAV9/3-SynI-GFP vector was employed, GFP expression was not observed in peripheral organs but was observed in peripheral neurons (Figures 2(g)–2(i)). The number of GFP/NeuN double-positive cells in the frontal cortex, hippocampus, and amygdala of yfAAV9/3-SynI-GFP vector-injected mice was counted and compared with that in yfAAV9/3-CAG-GFP vector-injected mice. The yfAAV9/3-SynI-GFP vector transduced approximately four times more neurons than the yfAAV9/3-CAG-GFP vector without transducing NeuN-negative nonneuronal cells (Figure 3). Furthermore, immunofluorescent examinations of spinal cord sections revealed GFP-IR motor neurons that also expressed the motor neuron marker choline acetyl transferase (ChAT) in the ventral horns (Figure 4).

To investigate if neuron-specific expression could also be obtained with other promoters, we generated yfAAV9/3 vectors where GFP was under control of the cerebellar Purkinje cell-specific L7 promoter [32]. As anticipated, the yfAAV9/3-L7-GFP vectors produced selective GFP expression in Purkinje cells (Figure 5).

3.3. Delivery of miRNAs into the Substantia Nigra. We next asked whether miRNAs could be delivered through systemic injections of the vectors into adult mice. We generated a yfAAV9/3 vector that expressed GFP and the pre-miRNA for AADC under control of the synapsin I promoter (yfAAV9/3-miR-AADC, Figure 6(a)). We administered the yfAAV9/3-miR-AADC vector (8.5×10^{12} vectors genome/mouse) to mice with intracardiac injections. Eight weeks after administration, mice were sacrificed, and we examined the expression of AADC, TH, and GFP in neurons of the substantia nigra pars compacta (SNc). Immunohistochemical examinations demonstrated extensive GFP-IR cells in the SNc (Figures 6(b) and 6(c)). AADC immunoreactivity was not detected in cells that expressed both GFP and TH (Figure 6(g), arrows). Furthermore, cells that were TH positive and GFP negative displayed AADC immunoreactivity (Figure 6(g), arrowheads). Taken together, these results suggest that we achieved selective inhibition of AADC expression in the transduced dopaminergic cells.

4. Discussion

The BBB is a significant obstacle when attempting to translate gene therapies for diseases that affect broad areas of the CNS.
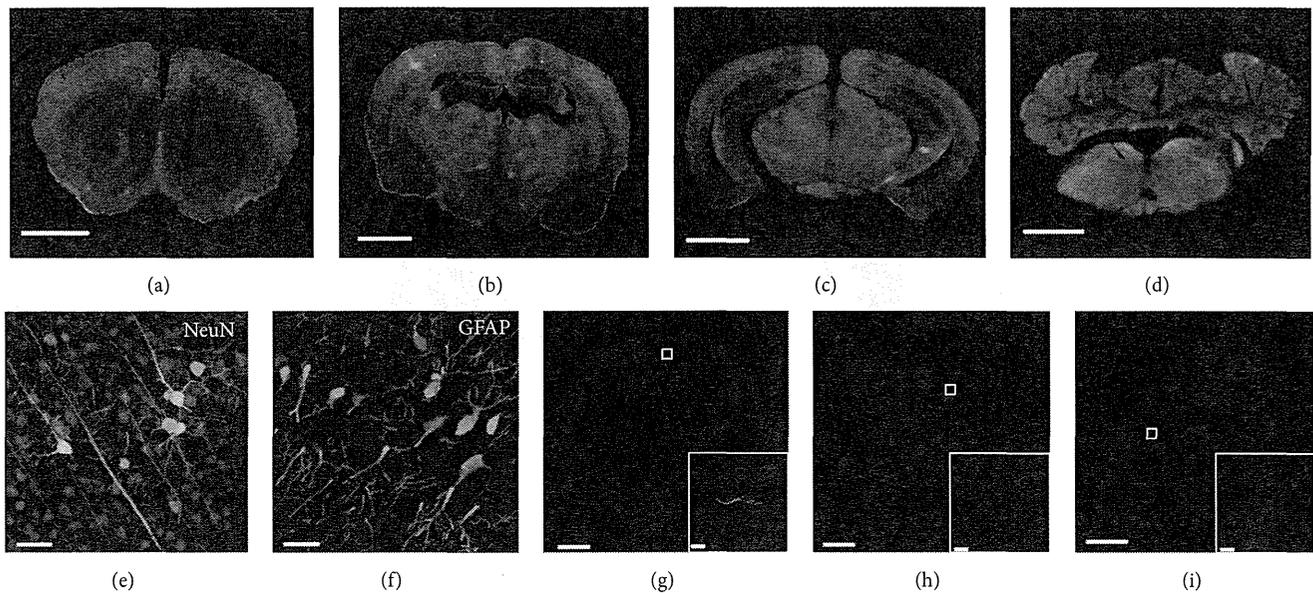
FIGURE 2: Efficient transduction of neurons with intracardiac injections of the tyrosine-mutant AAV9/3 vectors containing a neuron-specific promoter. Extensive transduction of neurons was achieved throughout the mouse brain by injections of tyrosine-mutant AAV9/3 vectors that expressed GFP under control of the synapsin I promoter. Representative images of coronal sections stained with an anti-GFP antibody following virus administration. Section locations relative to the Bregma: (a) +0.74 mm; (b) –1.82 mm; (c) –2.92 mm; and (d) –6.12 mm. ((e), (f)) Merged images showing results of double immunostaining experiments. Nearly all transduced cells were immunoreactive for NeuN but not GFAP. (e) GFP (green), NeuN (red); and (f) GFP (green), GFAP (red). Analysis of peripheral organs in yfAAV9/3-SynI-GFP vector-injected mice revealed that GFP expression was not observed in heart muscle, kidney cells, or hepatocytes ((g)–(i)) and was restricted to peripheral nerve cells (inset in (g)). Scale bars: ((a)–(d)) 2 mm; ((e), (f), and inset of (g)–(i)) 30 μm; ((g)–(i)) 1 mm.

We previously demonstrated that AAV8 vectors that were intravenously administered crossed the BBB and transduced both neurons and glial cells in adult mouse brains. Importantly, these mice had not been pre treated with any osmotic drugs [33]. A sizeable number of studies have focused on finding efficient and safe AAV vectors that can be used to deliver therapeutic genes to large areas of the CNS through systemic administrations. AAV9 vectors, especially double-stranded self-complementary AAV9 (scAAV9) vectors, administered through intravenous means can cross the BBB in mice [13, 16, 18], cats [10], and nonhuman primates [9, 14, 18] and achieve efficient gene delivery in the CNS. The advantage of scAAV9 vectors is that they bypass the need for conversion of the single-stranded AAV genome to double-stranded DNA and thus permit faster and increased expression of the transgene [17]. However, their small packaging capacity compromises the amount of genetic materials that can be inserted into the vectors. The inability to harbour large genes, promoters, and regulatory sequences is a significant disadvantage for many gene delivery applications [34]. Transduction of the CNS was also reported following intrathecal administration of scAAV9 vectors to nonhuman primates [9, 19] and pigs [11]. However, previous studies found that scAAV9 vectors have much greater infectivities of astrocytes than neurons in adult rodents [12, 35] and nonhuman primates [18]. Gene delivery to astrocytes has therapeutic potential for some neurological diseases, such as amyotrophic lateral sclerosis and Parkinson-disease, where astrocytes play active roles in neuronal survival [36, 37]. However, the relatively poor transduction of neurons limits the applications of AAV9 vectors.

Here, we demonstrated robust transductions of neurons in adult mice by systemic delivery of tyrosine-mutant AAV9/3 vectors with neuron-specific promoters. Surface-exposed tyrosine residues on AAV capsids are critical for infections. Oxidation of tyrosine residues hinders external-isation of the N-terminal portion of the capsid proteins [38]. Mutation of surface-exposed tyrosines to phenylala-nines reduces ubiquitination of the capsid proteins and improves the intracellular trafficking to the nucleus [39]. While enhanced gene deliveries to the retinas or spinal cords in mice are achieved with systemic administrations of single tyrosine-mutated AAV2, AAV8, and AAV9 [21, 40, 41], single tyrosine mutations in AAV8 and AAV9 capsids are insufficient for enhanced gene deliveries to the skeletal muscles and hearts [25]. Analyses of AAV2 vectors found that, of several different Y to F mutation combinations, a triple mutant vector (Y444, 500, and 730F) led to the most intense and uniform expression of transgenes in both cultured cells [22] and mice livers [42]. The amino acid residue at position 501 in wildtype AAV9 (residue 500 in AAV2) is phenylalanine, so we used a double tyrosine-mutant form of AAV9 (Y446F and Y731F) [26]. Neither mutation led to any sequence changes in the potential assembly activating protein (AAP) gene [43], and the mutant capsids packaged the vectors with titers similar to those of the wild-type capsids.
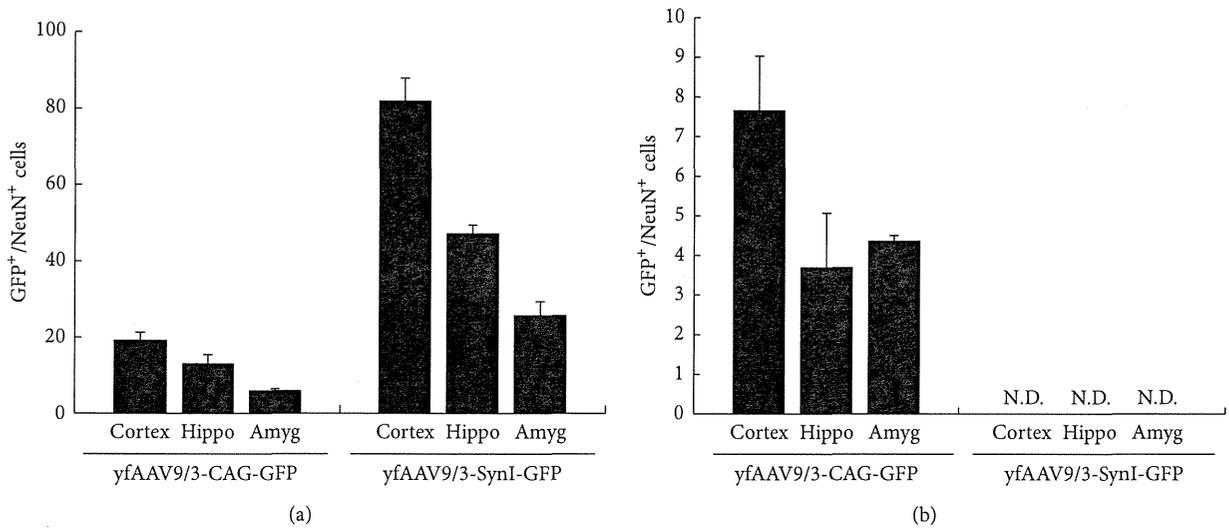
(a)

(b)

FIGURE 3: Quantification of neuronal transduction. The numbers of GFP$^+$/NeuN$^+$ neuronal or GFP$^+$/NeuN$^-$ nonneuronal cells in yfAAV-CAG-GFP-injected and yfAAV-SynI-GFP-injected mice ($n = 6$) were compared. The yfAAV9/3-SynI-GFP vector transduced approximately four times more NeuN-positive neurons than the yfAAV9/3-CAG-GFP vector in the frontal cortex, hippocampus, and amygdala. The volume of each region of interest was $0.04 \times 1 \times 1$ mm^3. A total of eight sections of each region of interest were analyzed. N.D., not detected; Hippo, hippocampus; Amyg, amygdala.
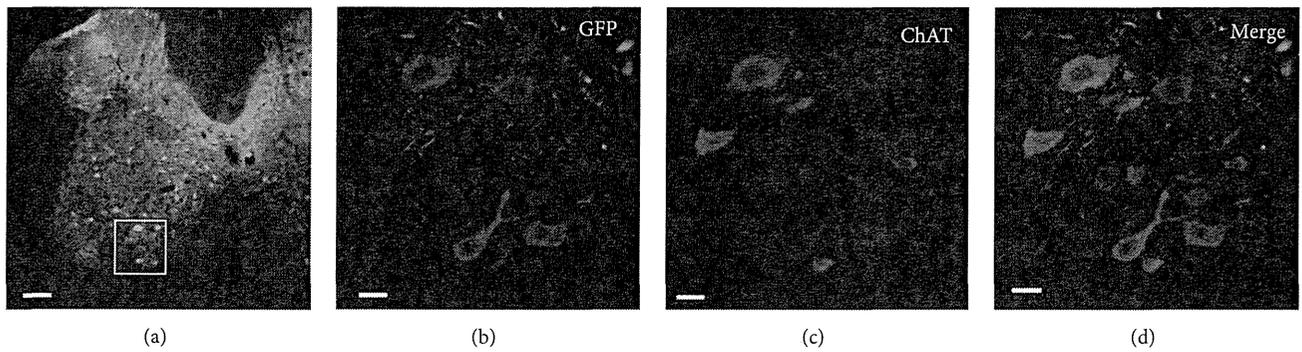

(a) (b) (c) (d)

FIGURE 4: Transduction of spinal cord motor neurons. Immunohistochemical detection of GFP and choline acetyl transferase (ChAT), a motor neuron marker, in mice spinal cords following intracardiac injections of tyrosine-mutant AAV9/3 vectors that expressed GFP under control of the synapsin I promoter. (a) An axial section demonstrating colabeling of GFP (green) and ChAT (red) in the large ventral horn neurons of the spinal cord. ((b)–(d)) High magnification images of the square area outlined in (a). (b) GFP-positive cells (green); (c) ChAT-positive cells (red); and (d) the merged image of ((b) and (c)). Scale bars: (a) 100 μm; ((b)–(d)) 20 μm.
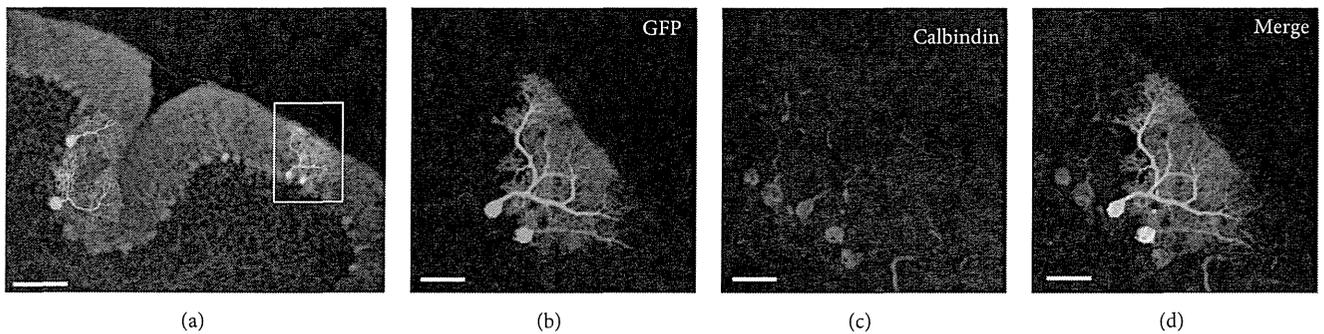

(a) (b) (c) (d)

FIGURE 5: Transduction of cerebellar Purkinje cells. Immunohistochemical detection of GFP and calbindin, a Purkinje cell marker, in mouse cerebellums following intracardiac injections of tyrosine-mutant AAV9/3 vectors that expressed GFP under control of the L7 promoter. (a) An axial section demonstrating colabeling of GFP (green) and calbindin (red) in the cerebellar cortex. ((b)–(d)) High magnification images of the rectangular area outlined in (a). (b) GFP-positive cells (green); (c) Calbindin-positive cells (red); and (d) the merged image of ((b) and (c)). Scale bars: (a) 100 μm; ((b)–(d)) 30 μm.
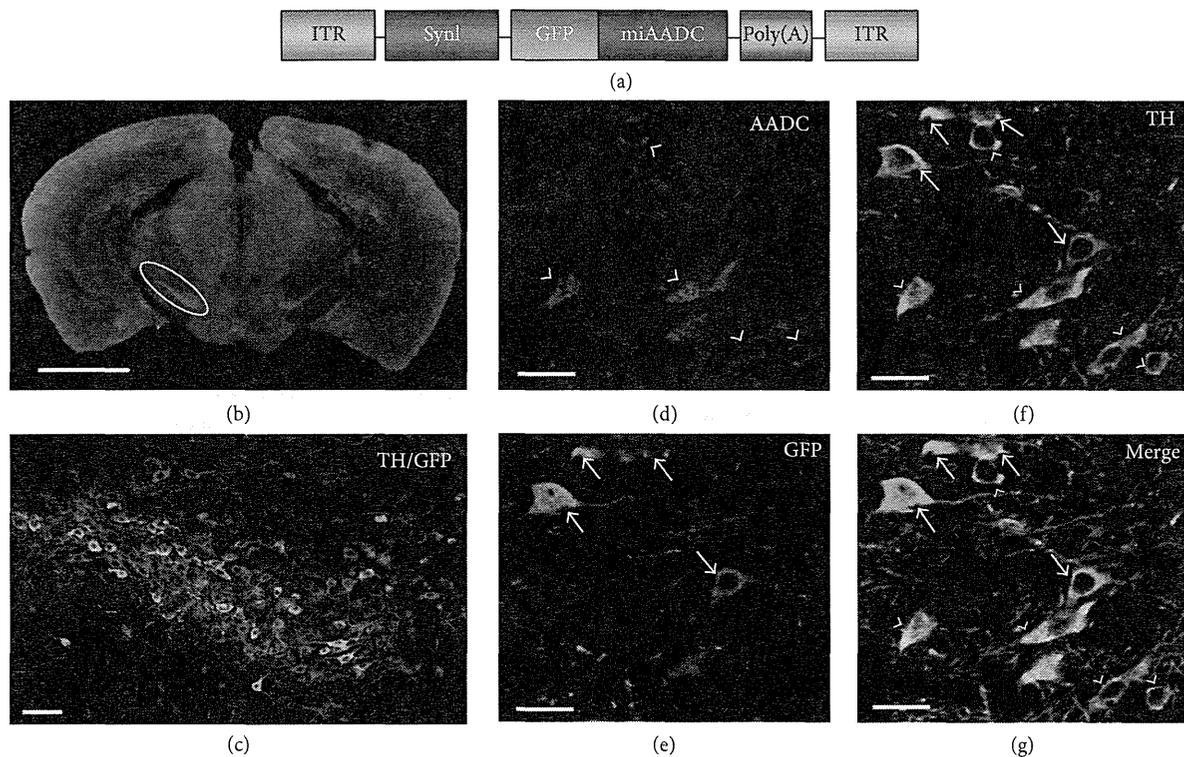
FIGURE 6: Delivery of miRNAs into the substantia nigra with systemic injections of tyrosine-mutant AAV9/3 vectors. (a) Illustration of the vector construct. The double-stranded pre-miRNA sequence for aromatic L-amino acid decarboxylase (AADC) was placed between the GFP and SV40 poly(A) sequences. ITR: inverted terminal repeat; SynI: synapsin I promoter. (b) A coronal mouse brain section showing a high concentration of GFP-immunoreactive cells in the substantia nigra pars compacta (SNc, circled area). (c) An enlarged image of the SNc subjected to double immunostaining shows colocalization of GFP-positive cells (green) and tyrosine hydroxylase (TH-) positive cells (red). ((d)-(g)) Selective inhibition of AADC expression in SNc neurons. AADC immunoreactivity (red) was not detected in the cells that were positive for both GFP (green) and TH (blue) (arrows). TH-positive cells that were GFP-negative displayed AADC immunoreactivity (arrowheads). Scale bars: (b) 2 mm; (c) 100 μm; ((d)-(g)) 20 μm.

Although the CAG promoter achieved extensive transgene expression in the mouse CNS, transduction of antigen-presenting cells with vectors containing ubiquitous promoters may trigger strong cell-mediated immune responses. However, generation of viral vectors with neuron-specific promoters will permit directed expression of therapeutic proteins in diseased neurons.

We targeted SNc neurons to determine whether yfAAV9/3 vectors are capable of functional miRNA delivery. The dopaminergic neurons in the SNc that express both TH and AADC are well defined and well characterised. We found that selective inhibition of AADC was possible with systemic injections of AAV vectors. This approach could provide a novel therapeutic strategy for future studies into Parkinson's disease or basal ganglia functions.

5. Conclusion

We showed that double tyrosine-mutant AAV9/3 vectors significantly enhanced gene delivery to the CNS and that viral-mediated gene expression can be restricted to neurons by incorporating neuron-specific promoters into viral vectors. This approach provides a new methodology for the future development of CNS gene therapies and creation of animal models of neurodegenerative diseases.

Conflict of Interests

All authors report no conflict of interests.

Acknowledgments

References

[1] W. J. Bowers, X. O. Breakefield, and M. Sena-Esteves, "Genetic therapy for the nervous system," Human Molecular Genetics, vol. 20, no. R1, pp. R28-R41, 2011.

[2] K. A. High and P. Aubourg, "rAAV human trial experience," *Methods in Molecular Biology*, vol. 807, pp. 429–457, 2011.

[3] M. S. Weinberg, R. J. Samulski, and T. J. McCown, "Adeno-associated virus (AAV) gene therapy for neurological disease," *Neuropharmacology*, vol. 69, pp. 82—88, 2013.

[4] P. Hadaczek, J. L. Eberling, P. Pivirotto, J. Bringas, J. Forsayeth, and K. S. Bankiewicz, "Eight years of clinical improvement in MPTP-lesioned primates after gene therapy with AAV2-hAADC," *Molecular Therapy*, vol. 18, no. 8, pp. 1458–1461, 2010.

[5] S. Muramatsu, K. Fujimoto, S. Kato et al., "A phase I study of aromatic L-amino acid decarboxylase gene therapy for parkinson's disease," *Molecular Therapy*, vol. 18, no. 9, pp. 1731–1735, 2010.

[6] R. T. Bartus, T. L. Baumann, L. Brown et al., "Advancing neurotrophic factors as treatments for age-related neurodegenerative diseases: developing and demonstrating, "clinical proof-of-concept" for AAV-neurturin (CERE-120) in Parkinson's disease," *Neurobiology of Aging*, vol. 34, no. 1, pp. 35–61, 2012.

[7] C. W. Christine, P. A. Starr, P. S. Larson et al., "Safety and tolerability of putaminal AADC gene therapy for Parkinson disease," *Neurology*, vol. 73, no. 20, pp. 1662–1669, 2009.

[8] P. A. LeWitt, A. R. Rezai, M. A. Leehey et al., "AAV2-GAD gene therapy for advanced Parkinson's disease: a double-blind, sham-surgery controlled, randomised trial," *The Lancet Neurology*, vol. 10, no. 4, pp. 309–319, 2011.

[9] A. K. Bevan, S. Duque, K. D. Foust et al., "Systemic gene delivery in large species for targeting spinal cord, brain, and peripheral tissues for pediatric disorders," *Molecular Therapy*, vol. 19, no. 11, pp. 1971–1980, 2011.

[10] S. Duque, B. Joussemet, C. Riviere et al., "Intravenous administration of self-complementary AAV9 enables transgene delivery to adult motor neurons," *Molecular Therapy*, vol. 17, no. 7, pp. 1187–1196, 2009.

[11] T. Federici, J. S. Taub, G. R. Baum et al., "Robust spinal motor neuron transduction following intrathecal delivery of AAV9 in pigs," *Gene Therapy*, vol. 19, no. 8, pp. 852–859, 2012.

[12] K. D. Foust, E. Nurre, C. L. Montgomery, A. Hernandez, C. M. Chan, and B. K. Kaspar, "Intravascular AAV9 preferentially targets neonatal neurons and adult astrocytes," *Nature Biotechnology*, vol. 27, no. 1, pp. 59–65, 2009.

[13] A. A. Rahim, A. M. Wong, K. Hoefer et al., "Intravenous administration of AAV2/9 to the fetal and neonatal mouse leads to differential targeting of CNS cell types and extensive transduction of the nervous system," *The FASEB Journal*, vol. 25, no. 10, pp. 3505–3518, 2011.

[14] L. Samaranch, E. A. Salegio, W. San Sebastian et al., "Adeno-associated virus serotype 9 transduction in the central nervous system of nonhuman primates," *Human Gene Therapy*, vol. 23, no. 4, pp. 382–389, 2012.

[15] J. J. Glascock, E. Y. Osman, M. J. Wetz et al., "Decreasing disease severity in symptomatic, Smn(−/−);SMN2(+/+), spinal muscular atrophy mice following scAAV9-SMN delivery," *Human Gene Therapy*, vol. 23, no. 3, pp. 330–335, 2012.

[16] K. D. Foust, X. Wang, V. L. McGovern et al., "Rescue of the spinal muscular atrophy phenotype in a mouse model by early postnatal delivery of SMN," *Nature Biotechnology*, vol. 28, no. 3, pp. 271–274, 2010.

[17] D. M. McCarty, "Self-complementary AAV vectors; advances and applications," *Molecular Therapy*, vol. 16, no. 10, pp. 1648–1656, 2008.

[18] S. J. Gray, V. Matagne, L. Bachaboina, S. Yadav, S. R. Ojeda, and R. J. Samulski, "Preclinical differences of intravascular AAV9 delivery to neurons and glia: a comparative study of adult mice and nonhuman primates," *Molecular Therapy*, vol. 19, no. 6, pp. 1058–1069, 2011.

[19] A. Ciesielska, P. Hadaczek, G. Mittermeyer et al., "Cerebral infusion of AAV9 vector-encoding non-self proteins can elicit cell-mediated immune responses," *Molecular Therapy*, vol. 21, no. 1, pp. 158–166, 2012.

[20] A. Delzor, N. Dufour, F. Petit et al., "Restricted transgene expression in the brain with cell-type specific neuronal promoters," *Human Gene Therapy Methods*, vol. 23, no. 4, pp. 242–254, 2012.

[21] C. A. Ku, V. A. Chiodo, S. L. Boye et al., "Gene therapy using self-complementary Y733F capsid mutant AAV2/8 restores vision in a model of early onset Leber congenital amaurosis," *Human Molecular Genetics*, vol. 20, no. 23, pp. 4569–4581, 2011.

[22] M. Li, G. R. Jayandharan, B. Li et al., "High-efficiency transduction of fibroblasts and mesenchymal stem cells by tyrosine-mutant AAV2 vectors for their potential use in cellular therapy," *Human Gene Therapy*, vol. 21, no. 11, pp. 1527–1543, 2010.

[23] H. Petrs-Silva, A. Dinculescu, Q. Li et al., "Novel properties of tyrosine-mutant AAV2 vectors in the mouse retina," *Molecular Therapy*, vol. 19, no. 2, pp. 293–301, 2011.

[24] C. Qiao, W. Zhang, Z. Yuan et al., "Adeno-associated virus serotype 6 capsid tyrosine-to-phenylalanine mutations improve gene transfer to skeletal muscle," *Human Gene Therapy*, vol. 21, no. 10, pp. 1343–1348, 2010.

[25] B. Cheng, C. Ling, Y. Dai et al., "Development of optimized AAV3 serotype vectors: mechanism of high-efficiency transduction of human liver cancer cells," *Gene Therapy*, vol. 19, no. 4, pp. 375–384, 2012.

[26] D. Dalkara, L. C. Byrne, T. Lee et al., "Enhanced gene delivery to the neonatal retina through systemic administration of tyrosine-mutated AAV9," *Gene Therapy*, vol. 19, no. 2, pp. 176–181, 2012.

[27] Y. Zhang and D. Duan, "Novel mini-dystrophin gene dual adeno-associated virus vectors restore neuronal nitric oxide synthase expression at the sarcolemma," *Human Gene Therapy*, vol. 23, no. 1, pp. 98–103, 2012.

[28] T. Dittgen, A. Nimmerjahn, S. Komai et al., "Lentivirus-based genetic manipulations of cortical neurons and their optical and electrophysiological monitoring *in vivo*," *Proceedings of the National Academy of Sciences of the United States of America*, vol. 101, no. 52, pp. 18206–18211, 2004.

[29] O. Meyuhas and A. Klein, "The mouse ribosomal protein L7 gene. Its primary structure and functional analysis of the promoter region," *Journal of Biological Chemistry*, vol. 265, no. 20, pp. 11465–11473, 1990.

[30] G. Gao, L. H. Vandenberghe, M. R. Alvira et al., "Clades of adeno-associated viruses are widely disseminated in human tissues," *Journal of Virology*, vol. 78, no. 12, pp. 6381–6388, 2004.

[31] X. G. Li, T. Okada, M. Kodera et al., "Viral-mediated temporally controlled dopamine production in a rat model of Parkinson disease," *Molecular Therapy*, vol. 13, no. 1, pp. 160–166, 2006.

[32] W. Wagner, S. McCroskery, and J. A. Hammer III, "An efficient method for the long-term and specific expression of exogenous cDNAs in cultured Purkinje neurons," *Journal of Neuroscience Methods*, vol. 200, no. 2, pp. 95–105, 2011.

[33] H. Nakai, S. Fuess, T. A. Storm, S. I. Muramatsu, Y. Nara, and M. A. Kay, "Unrestricted hepatocyte transduction with adeno-associated virus serotype 8 vectors in mice," *Journal of Virology*, vol. 79, no. 1, pp. 214–224, 2005.

[34] Y. Wang, C. Ling, L. Song et al., "Limitations of encapsidation of recombinant self-complementary adeno-associated viral genomes in different serotype capsids and their quantitation," *Human Gene Therapy Methods*, vol. 23, no. 4, pp. 225–233, 2012.

[35] H. Zhang, B. Yang, X. Mu et al., "Several rAAV vectors efficiently cross the blood-brain barrier and transduce neurons and astrocytes in the neonatal mouse central nervous system," *Molecular Therapy*, vol. 19, no. 8, pp. 1440–1448, 2011.

[36] T. Philips and W. Robberecht, "Neuroinflammation in amyotrophic lateral sclerosis: role of glial activation in motor neuron disease," *The Lancet Neurology*, vol. 10, no. 3, pp. 253–263, 2011.

[37] P. M. Rappold and K. Tieu, "Astrocytes and therapeutics for Parkinson's disease," *Neurotherapeutics*, vol. 7, no. 4, pp. 413–423, 2010.

[38] E. D. Horowitz, M. G. Finn, and A. Asokan, "Tyrosine cross-linking reveals interfacial dynamics in adeno-associated viral capsids during infection," *ACS Chemical Biology*, vol. 7, no. 6, pp. 1059–1066, 2012.

[39] L. Zhong, B. Li, C. S. Mah et al., "Next generation of adeno-associated virus 2 vectors: point mutations in tyrosines lead to high-efficiency transduction at lower doses," *Proceedings of the National Academy of Sciences of the United States of America*, vol. 105, no. 22, pp. 7827–7832, 2008.

[40] H. Petrs-Silva, A. Dinculescu, Q. Li et al., "High-efficiency transduction of the mouse retina by tyrosine-mutant AAV serotype vectors," *Molecular Therapy*, vol. 17, no. 3, pp. 463–471, 2009.

[41] Y. Miyazaki, H. Adachi, M. Katsuno et al., "Viral delivery of miR-196a ameliorates the SBMA phenotype via the silencing of CELF2," *Nature Medicine*, vol. 18, no. 7, pp. 1136–1141, 2012.

[42] D. M. Markusic, R. W. Herzog, G. V. Aslanidi et al., "High-efficiency transduction and correction of murine hemophilia B using AAV2 vectors devoid of multiple surface-exposed tyrosines," *Molecular Therapy*, vol. 18, no. 12, pp. 2048–2056, 2010.

[43] M. Naumer, F. Sonntag, K. Schmidt et al., "Properties of the adeno-associated virus assembly activating protein," *Journal of Virology*, vol. 86, no. 23, pp. 13038–13048, 2012.

SCIENTIFIC REPORTS
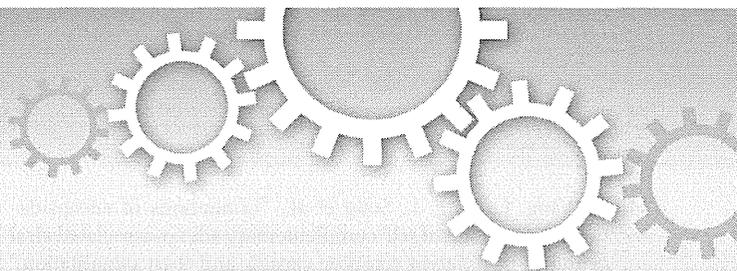
Global brain delivery of neprilysin gene by intravascular administration of AAV vector in mice

Nobuhisa Iwata[1,2], Misaki Sekiguchi[1], Yoshino Hattori[2], Akane Takahashi[2], Masashi Asai[2], Bin Ji[3], Makoto Higuchi[3], Matthias Staufenbiel[4], Shin-ichi Muramatsu[5] & Takaomi C. Saido[1]

[1]Laboratory for Proteolytic Neuroscience, RIKEN Brain Science Institute, 2-1 Hirosawa, Wako-shi, Saitama 351-0198, Japan, [2]Laboratory of Molecular Biology and Biotechnology, Department of Molecular Medicinal Sciences, Graduate School of Biomedical Sciences, Nagasaki University, 1-14 Bunkyo-machi, Nagasaki-shi, Nagasaki 852-8521, Japan, [3]Molecular Imaging Center, National Institute of Radiological Sciences, 4-9-1 Anagawa, Inage-ku, Chiba-shi, Chiba 263-8555, Japan, [4]Novartis Institutes for Biomedical Research, 4002 Basel, Switzerland, [5]Division of Neurology, Department of Medicine, Jichi Medical University, 3311-1 Yakushiji, Shimotsuke-shi, Tochigi 329-0498, Japan.

Accumulation of amyloid-β peptide (Aβ) in the brain is closely associated with cognitive decline in Alzheimer's disease (AD). Stereotaxic infusion of neprilysin-encoding viral vectors into the hippocampus has been shown to decrease Aβ in AD-model mice, but more efficient and global delivery is necessary to treat the broadly distributed burden in AD. Here we developed an adeno-associated virus (AAV) vector capable of providing neuronal gene expression throughout the brains after peripheral administration. A single intracardiac administration of the vector carrying neprilysin gene in AD-model mice elevated neprilysin activity broadly in the brain, and reduced Aβ oligomers, with concurrent alleviation of abnormal learning and memory function and improvement of amyloid burden. The exogenous neprilysin was localized mainly in endosomes, thereby effectively excluding Aβ oligomers from the brain. AAV vector-mediated gene transfer may provide a therapeutic strategy for neurodegenerative diseases, where global transduction of a therapeutic gene into the brain is necessary.

A ggregation and deposition of amyloid-β peptide (Aβ) in the brain are triggering events of the long-term pathological cascade of Alzheimer's disease (AD), and are closely associated with the metabolic balance between Aβ anabolic and catabolic activities[1,2]. As almost all familial AD mutations cause an increase in the anabolism of a particular form of Aβ, Aβ_{1-42}, leading to Aβ deposition and accelerating AD pathology, a chronic reduction in the catabolic activity would also promote Aβ deposition[1,2]. Neprilysin (EC 3.4.24.11) is a rate-limiting peptidase involved in brain Aβ catabolism, as proven by *in vivo* experiments tracing the catabolism of radiolabeled Aβ in brain and by reverse genetics studies for candidate peptidases in mice[3,4]. Neprilysin gene-disruption caused a gene dosage-dependent elevation of endogenous Aβ levels in mouse brain, suggesting that a subtle but long-term reduction in neprilysin activity would contribute to AD development by promoting accumulation of Aβ^2.

Mounting evidence that expression levels of neprilysin are decreased in the hippocampus and cerebral cortex of AD patients from the early stages of disease development and also with aging in humans, as well as mice, suggests a close association of neprilysin with the etiology and pathogenesis of AD[2]. Indeed, reduced activity of neprilysin in mouse brain elevates the levels of highly toxic Aβ oligomers at the synapses, and leads to impaired hippocampal synaptic plasticity and cognitive function even before apparent amyloid deposition is observed in the brain[5]. Thus, a decline in neprilysin activity appears to be at least partly responsible for the memory-related symptoms of AD, and up-regulation of neprilysin is considered to be a promising strategy for therapy and prevention of AD.

Experimental gene therapy to transfer neprilysin gene into the brains of AD model mice has been reported, and for this purpose various kinds of recombinant viral vectors carrying wild-type neprilysin or its variants that are truncated at the transmembrane region and can be released to extracellular space have been utilized[6,7]. Viral vector-mediated delivery of neprilysin gene successfully retarded amyloid deposition in the brains of AD model mice[6,7]. Beneficial potential of gene therapy has also been shown in other neurodegenerative diseases, including Parkinson's disease (PD). Gene transfer of dopamine-synthesizing enzymes into the putamen alleviated motor

166

1

symptoms in PD patients[8,9]. However, infusion of viral vectors via stereotaxic surgery is not necessarily appropriate if the therapeutic gene should be delivered to broad areas of the brain.

In this study we have successfully developed a new gene delivery system by employing the combination of rAAV9 with a neuron-specific promoter, and we have shown that this system can provide functional gene expression throughout the brains of mice after intracardiac administration. The AAV vector can achieve comprehensive gene expression of neprilysin in the brain of young neprilysin-deficient mice, eventually decelerating Aβ accumulation and alleviating cognitive dysfunction based on a water maze test in aged APP transgenic (tg) mice. We show that the majority of the exogenous neprilysin is localized in late and early endosomes, where newly generated Aβ is concentrated, and this may be the reason why Aβ can be effectively excluded from the brain.
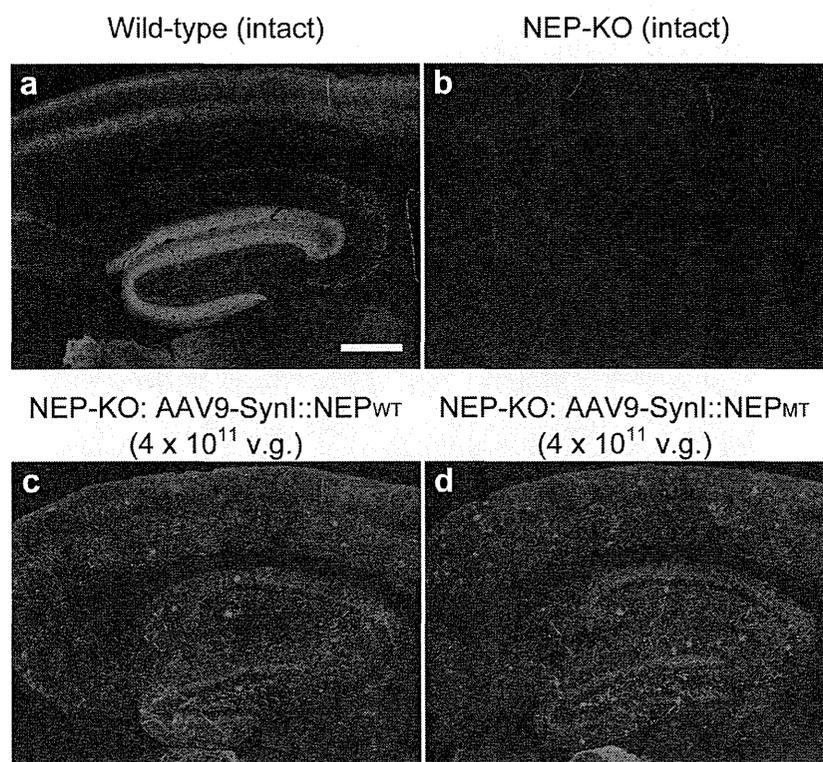
Results

Expression profile of neprilysin in the brain after AAV-mediated gene transfer. To deliver an AAV vector from circulating blood to the brain, we employed intracardiac administration, i.e., injection into the left ventricle of the heart, because this provides a direct route to the brain. To evaluate gene expression of neprilysin, we injected rAAV9 vectors that encode either an active or an inactive form of neprilysin in neprilysin-deficient mice[10] and examined the outcome by means of specific immunochemical staining for neprilysin. This staining generated specific signals of endogenous neprilysin in wild-type mice, but not in neprilysin-deficient mice without vector treatment (Fig. 1a,b). Expression of exogenous neprilysin after a single injection of rAAV9-NEP vector (4×10^{11} vector genome [v.g.]) into the left ventricle of the heart of neprilysin-deficient mice was spread over the limbic region on the neprilysin-null background (Fig. 1c,d), and presented a scattered distribution, but with locally intense signals. The total amount of exogenous neprilysin expression was dependent on amount of vector injected

into the mice over a range of 0.5–4.0×10^{11} v.g., as far as we examined (data not shown). On the other hand, intracardiac administration of rAAV9-NEP vector did not cause prominent gene expression of neprilysin in heart, lung, kidney or liver (Supplementary Fig. 1).

Next, we examined the localization of neprilysin in the brain by confocal double immunostaining for neprilyin and several marker proteins, after the injection of rAAV9-NEP vector into neprilysin-deficient mice. Neprilysin was present in vesicular structures of NeuN-positive neurons (Fig. 2a–c), but not in glial fibrillary acidic protein (GFAP)-positive astrocytes (data not shown). In addition, we found that exogenous neprilysin is colocalized with late endosomal marker proteins Ras-related protein 7 (Rab7) (Fig. 2d–f) and Rab9 (Fig. 2g–i), and also in part with early endosomal markers Rab5 (Fig. 2j–l) and early endosome antigen 1 protein (EEA1) (Fig. 2m–o), but not with presynaptic markers SV2 (Fig. 2p–r) and syntaxin 1, secretory vesicle marker Rab3a, clathrin-coated vesicle marker clathrin heavy chain, somato-dendritic marker microtubule-associated protein 2 (MAP2), or postsynaptic marker PSD-95 (data not shown).
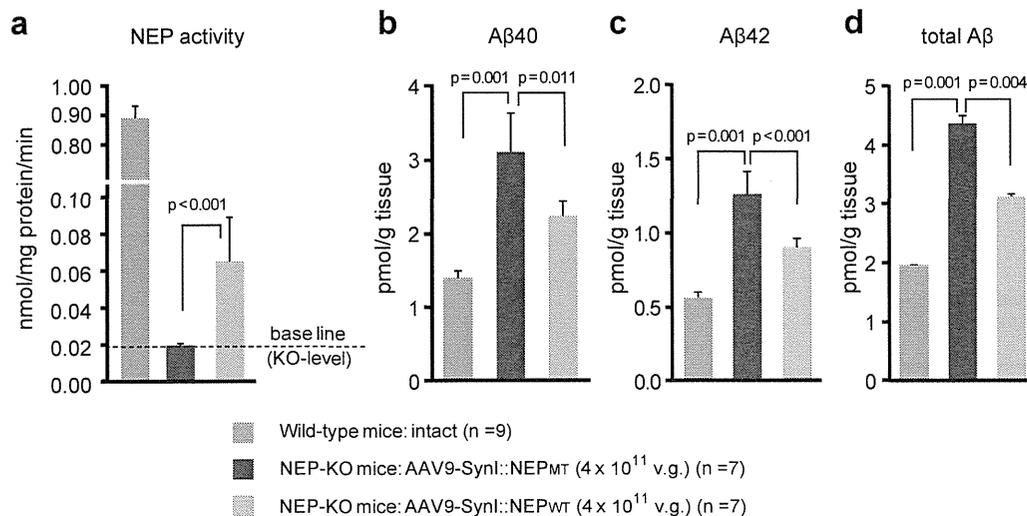
Functional expression of neprilysin. We investigated functional expression of neprilysin and subsequent reduction of Aβ levels in the brain. Four weeks after the single intracardiac injection of rAAV-NEP_WT vector into neprilysin-deficient mice, neprilysin activity in the limbic region including the neocortex and hippocampus was significantly increased compared to that after injection of rAAV-NEP_MT vector, although the increased level of neprilysin activity was less than 10% of the level observed in intact wild-type mice (Fig. 3). The injection of rAAV-NEP_WT vector into neprilysin-deficient mice significantly reduced Aβ40, Aβ42 and total Aβ levels in the limbic region compared to those in the mice injected with rAAV-NEP_MT. The partially compensated neprilysin activity was sufficient to achieve a 50% reduction of the elevated Aβ levels in the neprilysin-deficient mice.

Wild-type (intact)　　　NEP-KO (intact)

NEP-KO: AAV9-SynI::NEP_WT (4×10^{11} v.g.)　　NEP-KO: AAV9-SynI::NEP_MT (4×10^{11} v.g.)

Figure 1 | Intracardiac injection of rAAV9 with SynI promoter leads to widespread gene transduction of neprilysin in the brain. Brain sections from intact wild-type mice (a), intact neprilysin-deficient mice (b), and neprilysin-deficient mice 14 days after intracardiac injection of 4×10^{11} genome vectors of rAAV9-SynI::NEP_WT (c) or rAAV9-SynI::NEP_MT (d). Scale bars, 200 μm.

167
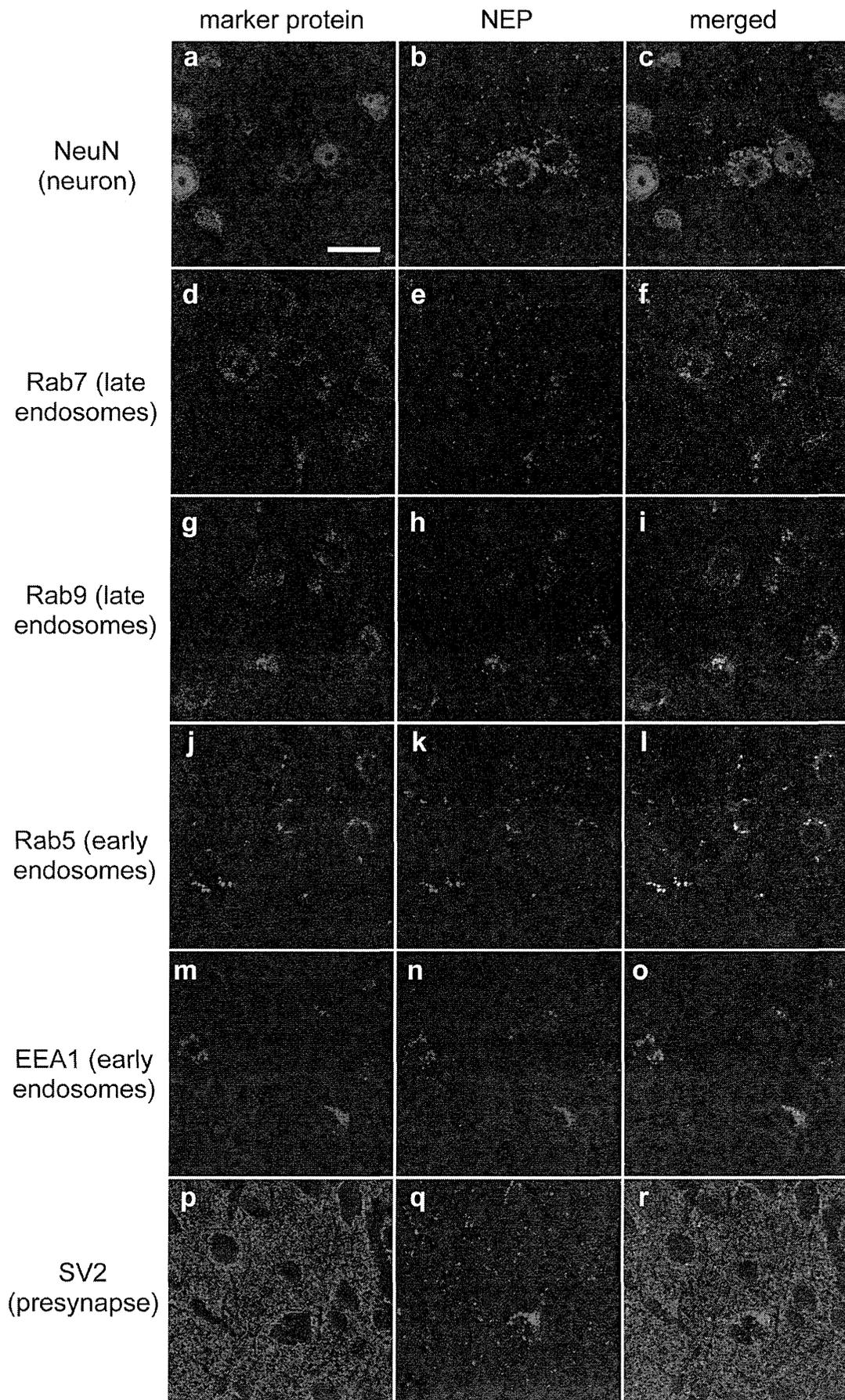
Figure 2 | Localization of the exogenous neprilysin in the brain. Brain sections from neprilysin-knockout mice 14 days after intracardiac injection of 4×10^{11} genome vectors of rAAV9-SynI::NEP$_{WT}$. Exogenous neprilysin was localized in NeuN-positive neurons (a–c), and was also observed in endosomes as confirmed by colocalization with Rab7 (d–f), Rab9 (g–i), Rab5 (j–l), EEA1 (m–o), and SV2 (p–r). Scale bars, 20 μm.

168

Figure 3 | Functional expression of NEP and Aβ levels in the limbic region after gene transfer. (a) Levels of neprilysin-dependent endopeptidase activity in the limbic regions of intact wild-type, rAAV9-SynI::NEP$_{MT}$- and rAAV-SynI::NEP$_{WT}$-injected NEP-KO mice 14 days after intracardiac injection. Data represent mean ± s.e.m. of 7–9 mice. (b–d) Levels of Aβ40, Aβ42 and total Aβs in the limbic regions after the gene transfer were determined by sandwich ELISA. A non-specific reaction of the ELISA system was excluded by subtracting values obtained in the brain tissue from APP-KO mice. Data represent mean ± s.e.m. of 7–9 mice.

Rescue of aged mutant APP tg mice from Aβ accumulation and subsequent impairment of memory and learning function. We next investigated the potential of intracardiac injection of rAAV9 vector to reverse the impaired memory and learning function in mutant APP tg mice (APP23)[11]. Since Aβ production in APP23 mice is about 10-fold higher than that of wild-type mice, a nearly 4-fold higher dose of vector was used than in the above-mentioned treatment of neprilysin-deficient mice. We examined reference memory as an indication of spatial memory and learning function, using a Morris water maze task. Under our experimental conditions, impairment of reference memory function of mutant APP tg mice was detected at the age of 15 months (Fig. 4a), and so we randomly divided mice of this age into two groups, which were given intracardiac administration of rAAV9-NEP$_{MT}$ or rAAV-NEP$_{WT}$. Five months after the gene transfer, we re-examined their memory functions. The escape latency of rAAV9-NEP$_{WT}$-injected APP tg mice was significantly shorter than that of rAAV9-NEP$_{MT}$-injected mice (*p < 0.05), in which the escape latency was not shortened at all and the learning and memory function remained impaired (Fig. 4b). The cognitive function of the rAAV9-NEP$_{WT}$-injected APP tg mice was restored nearly to the level of intact wild-type mice. In addition, it is reported that anxiety-like behaviors affect performance in spatial learning tasks[12], and we cannot rule out the possibility that the effect of neprilysin gene transfer involved, at least in part, alleviation of anxiety-like behaviors that might have been exacerbated by the amyloid burden.

Next, we assessed plaque deposition and glial activation in the brains of rAAV9-injected APP tg mice by positron emission tomography (PET) with radioligands for amyloid (Pittsburgh Compound-B [11C]PIB) and 18-kDa translocator protein (TSPO) ([11C]Ac5216), respectively (Fig. 4c,d)[13,14]. Plaque deposition in both the hippocampus and neocortex was clearly reduced in the rAAV9-NEP$_{WT}$-injected mice compared to rAAV9-NEP$_{MT}$-injected mice (*p < 0.05). Mice treated with rAAV9-NEP$_{WT}$ showed a tendency of enhanced TSPO upregulation, and the TSPO/amyloid burden ratio was significantly different between the two treatment groups (*p < 0.05). This observation is attributable to reinforcement of TSPO-positive, neuroprotective astrogliosis surrounding Aβ plaques[15]. Thus, in vivo assessments supported the potential effectiveness of gene therapy by intracardiac administration of rAAV9-NEP$_{WT}$ in a pathological animal model.

Therapeutic effects of NEP gene transfer on Aβ pathologies in the brain. After PET imaging analysis (i.e., 6 months after the gene transfer), functional expression of neprilysin was estimated by measurement of enzyme activity using a standard fluorescent substrate, and amyloid deposition was assessed by immunohistochemical staining using specific antibodies against either the unmodified amino-terminus of Aβ, N1D, or the modified amino-terminus of Aβ, N3pE[16]. Neprilysin-dependent endopeptidase activity in both the hippocampus and the neocortex maintained a 1.5-fold increase in the rAAV9-NEP$_{WT}$-injected mice compared to that in rAAV9-NEP$_{MT}$-injected mice (*p < 0.05) (Fig. 5a), and both N1D- and N3pE-positive amyloid deposits were consistently and significantly decreased (*p < 0.05) (Fig. 5b,c).

We further investigated membrane-associated Aβ oligomers, which were extracted with Triton X-100 from the membrane fraction, using western blotting (Fig. 5d,e). Membrane-associated Aβs were detected as oligomers, consisting mainly of trimers/tetramers, followed by dimer, and with only a trace of monomer. The Aβ trimers/tetramers, which were not detected from non-tg (wild-type) mouse brain, were significantly decreased by the rAAV9-NEP$_{WT}$ administration (20% reduction; *p < 0.05), compared to that in the rAAV9-NEP$_{MT}$ group. According to the current hypothesis that Aβ oligomers are the primary molecules responsible for cognitive dysfunction, rather than Aβ fibrils[17-19], the reduction of Aβ oligomers following rAAV9-NEP$_{WT}$ administration may contribute directly to the alleviation of abnormal spatial learning and memory function in aged mutant APP tg mice.

Discussion

Recombinant AAV vectors are among the most promising vehicles for gene delivery to the central nervous system. Stereotaxic infusion of AAV vector carrying neprilysin gene into the hippocampus has been shown to decrease Aβ in AD model mice[6,7]. However, when it was infused into the neocortex or hippocampal formation, expression of exogenous neprilysin and its effects on Aβ degradation were locally restricted[6,7]. Since the extent of the Aβ burden is broad in AD, a more efficient and widespread delivery technology is necessary. Among more than one hundred primate AAVs, AAV9 has gained much attention, showing high efficiency of gene transduction in neurons after intravenous administration in neonatal mice[20]. Here

169
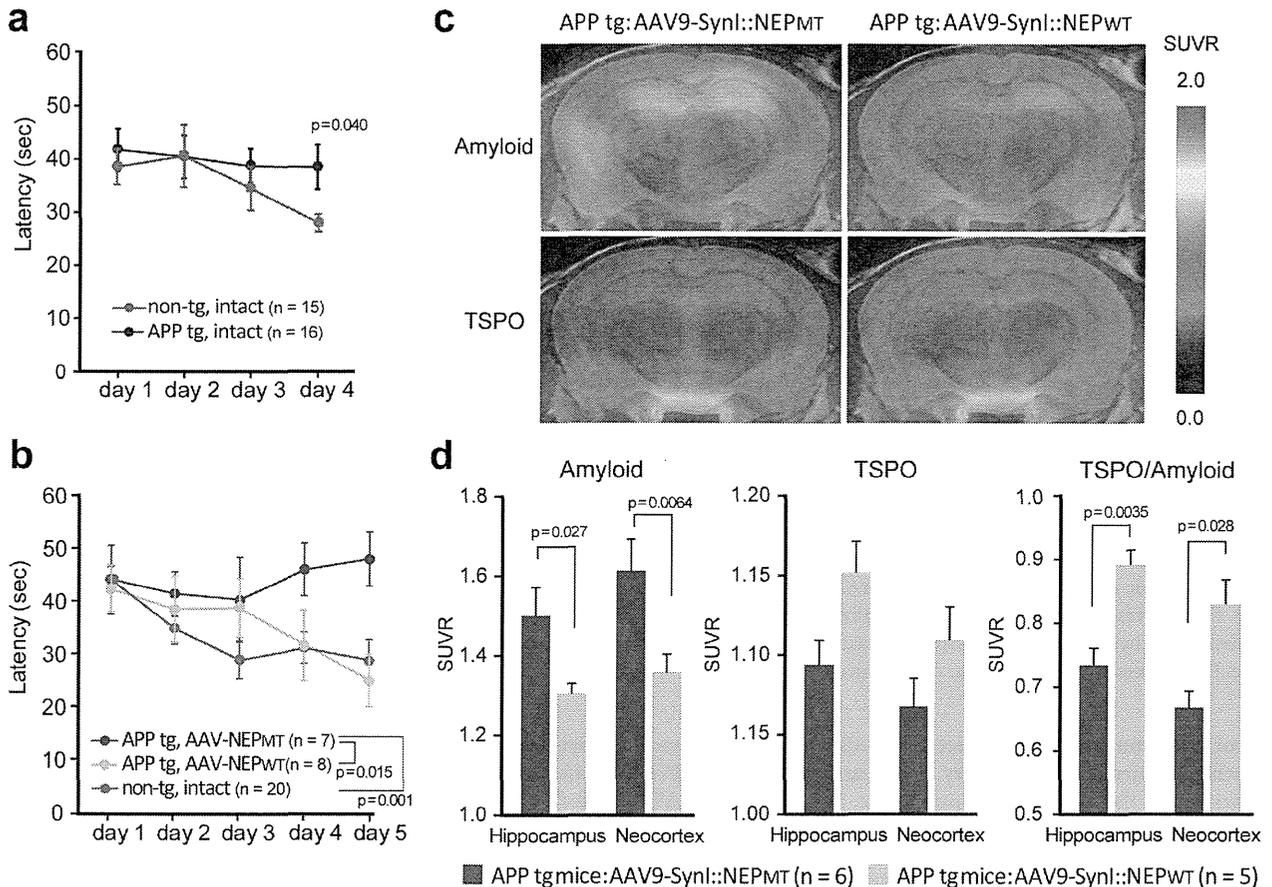
Figure 4 | NEP gene transfer ameliorated impaired spatial learning and memory function, amyloid burden, and modified glial activation in aged APP tg mice. Reference memory was examined using a water maze task. Escape latency in each block to the hidden platform during a 60-sec session was measured. (a) Impaired reference memory function of APP tg mice at the ages of 15 months was detected, and they were divided into two groups, followed by administration of AAV9-SynI::NEP$_{MT}$ or AAV9-SynI::NEP$_{WT}$ (1.5 × 10^{12} genome copies). Data represent mean ± s.e.m. (b) Five months after the gene transfer, their memory functions were re-examined. Two-way ANOVA showed a significant main effect of neprilysin gene transfer ($F_{(2,160)}$ = 6.287; $p < 0.05$). Post hoc analysis revealed that the escape latency of rAAV9-SynI::NEP$_{MT}$-injected APP tg mice was significantly different from the other groups ($p < 0.05$). Data represent mean ± s.e.m. (c) Plaque deposition and glial activation in living brains of APP tg mice 5 months after injection of AAV9-SynI::NEP$_{MT}$ and AAV9-SynI::NEP$_{WT}$ assessed by PET with radioligands for amyloid ([^{11}C]PIB) (top) and TSPO ([^{11}C]Ac5216) (bottom). Amyloid and TSPO images are derived from the same individuals. Data represent mean ± s.e.m. (d) The levels were estimated as SUVRs. TSPO upregulation relative to amyloid abundance was also determined by calculating the quotient of the SUVRs for [^{11}C]Ac5216 and [^{11}C]PIB (right). The main effect of the treatment was significant on amyloid load ($F_{(1,12)}$ = 9.17, $p < 0.05$) and TSPO-to-amyloid ratio ($F_{(1,10)}$ = 16.4, $p < 0.01$) but insignificant on TSPO level ($F_{(1,10)}$ = 4.2, $p > 0.05$) by repeated-measures 2-way ANOVA. The p values show significant differences between rAAV9-SynI::NEP$_{WT}$ and rAAV-SynI::NEP$_{WT}$. Data represent mean ± s.e.m.

we showed that intracardiac administration of AAV9 can deliver neprilysin gene into broad areas of the adult mouse brain, and results in a marked and widespread reduction of Aβ levels. Although the mechanism by which AAV9 penetrates the blood-brain barrier (BBB) remains unknown, tyrosine mutation of the adeno-associated viral capsid protein may contribute to the enhanced expression levels of transgenes delivered by AAV[21].

It is noteworthy that a relatively small increase of neprilysin activity in the brain was sufficient to yield a significant reduction of Aβ, with subsequent alleviation of abnormal spatial learning and memory function. The exogenous neprilysin was abundantly present in late and early endosomes of neurons throughout the brain, including the neocortex and hippocampal formation. This localization appears to provide a rationale for the effective degradation of Aβ, as discussed below. It is considered that Aβ is generated in late endosomes, then is secreted from presynaptic terminals of neurons by neuronal activity-dependent exocytosis[22], and is temporally concentrated and may be oligomerized/aggregated. In addition, Walsh et al. reported that Aβ oligomerization occurred after generation of the peptide within specific intracellular vesicles including recycling endosomes[23], which

could be modulated by Aβ per se[24], and the oligomers are subsequently secreted from the cell. This observation is supported by the fact that the mildly acidic environment (pH 5 ~ 6) in endosomes appears to promote Aβ oligomerization/aggregation[25]. After this event, Aβ or Aβ oligomers impair neuronal transmission via binding to N-methyl-D-aspartic acid (NMDA) or acetylcholine α7 nicotinic (α7nACh) receptors and prion protein[17–19]. Aβ/Aβ oligomers are diffused in the synaptic clefts after secretion, but they maintain a higher concentration in endosomal membrane, and may also be tethered in part at the plasma membrane. Although neprilysin is a neutral endopeptidase, its pH optimum is around 6.0[26], so neprilysin could degrade Aβ oligomers efficiently under the mildly acidic conditions in endosomes.

We succeeded in excluding membrane-associated Aβ oligomers from the brain by means of neprilysin gene transfer, ameliorating the impairment of spatial learning and memory function, although the contribution of a reduction in the total amount of amyloid deposition cannot be neglected. However, mounting evidence suggests that Aβ oligomers are highly neurotoxic[17–19] and may be more directly responsible for the pathological and symptomatic changes in AD,

170
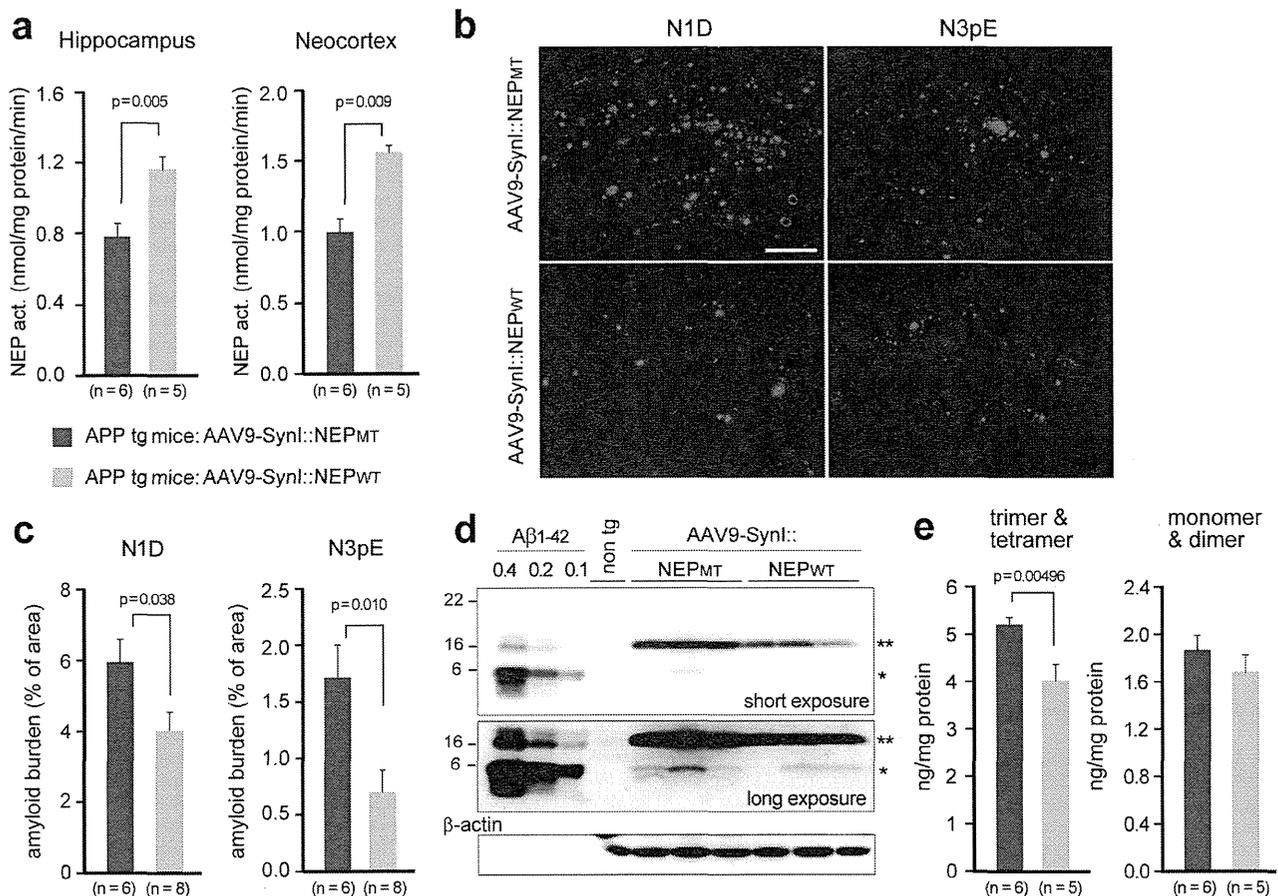
Figure 5 | Gene therapeutic effects of NEP gene transfer on Aβ pathologies in the brains. Seven months after the gene transfer into 15-month-old APP tg mice, brains were removed and analyzed biochemically and immunohistochemically. (a) NEP activities in the hippocampal formation and neocortex. (b) Amyloid burden. Brain sections were immunostained with N-terminal specific antibodies for Aβ (N1D and N3pE, mouse monoclonal). Scale bar, 500 μm. (c) Amyloid load is expressed as percent of the measured area. Data represent mean ± s.e.m. The p values show significant differences between rAAV9-SynI::NEP_{MT} and rAAV-SynI::NEP_{WT}. (d) A representative blot of Aβ and its oligomers. Triton X-100-extractable membrane fractions (20 μg protein) from the hippocampal formation of APP tg mice with rAAV9-NEP_{MT} or rAAV9-NEP_{WT} and non-transgenic (wild type) mice were subjected to western blot analyses using N-terminal specific antibody N1D (rabbit polyclonal). A single asterisk shows Aβ dimer, and a double asterisk shows trimer and tetramer. The blot was reprobed with anti-β-actin antibody. (e) Aβ oligomers in the blots were quantified by densitometry. Synthetic Aβ$_{1-42}$ (0.1, 0.2, 0.4 ng) run on the same gel as indicated in d was used for calibration within a linear range. The p values show significant differences between rAAV9-SynI::NEP_{MT} and rAAV-SynI::NEP_{WT}. Data represent mean ± s.e.m.

such as synaptic dysfunction and subsequent cognitive dysfunction[27]. This concept appears to be reinforced by a lesson from the failure of a clinical trial of Aβ vaccine[28], and thus supports the notion that reduction in neprilysin-sensitive and membrane-associated Aβ oligomers may be the key factor in the alleviation of cognitive impairment.

Aβ that accumulates and forms amyloid plaques in AD brain consists mostly of amino-terminally truncated and modified Aβ, AβN3pE[16], and this implies that Aβ secreted from neurons undergoes posttranslational modifications in the process of plaque formation. Although this fact has been known for decades, this specific form of Aβ, AβN3pE, has become of interest again since it was reported that PIB probe recognized AβN3pE with higher affinity than it did amino-terminally intact Aβ$_{1-42}$[13]. AβN3pE is more hydrophobic and more easily self-aggregated (250-fold) than Aβ$_{1-42}$[29], and is more resistant to proteolytic degradation (by 4-fold) (Iwata and Saido, unpublished data). Recently, it was reported that AβN3pE could be a seed for oligomerization/aggregation, and showed more potent neurotoxicity than AβN1D[30]. Schilling, et al. reported that administration of a synthetic inhibitor specific to glutaminyl cyclase (QC), which is involved in cyclization of the third glutamate residue of Aβ, reduced not only production of AβN3pE, but also the total

amount of amyloid deposition, and it also alleviated cognitive impairment in AD-model mice (Tg2576)[31]. In this study, we found that the gene transfer abolished any increase in amyloid fibrils composed of AβN3pE, as well as amino-terminally intact Aβ, in the brains of aged APP tg mice (APP23). This result may be attributed to degradation of newly produced Aβ by exogenous neprilysin in endosomes, rather than direct degradation of AβN3pE. Because AβN3pE acquires proteolytic resistance once it is formed from Aβ$_{1-x}$, Aβ degradation in endosomes immediately after its production should be favorable for efficient degradation. This notion appears to be supported by the finding that we could not detect AβN3pE or its oligomeric forms in the membrane fraction (i.e., their concentrations were below the detection limit of western blot analysis)(data not shown).

Therapeutic intervention by neprilysin gene transfer could be monitored *in vivo* by using microPET with [^{11}C]PIB probe. TSPO is a marker protein in activated glias, such as astrocytes and microglias. Ji et al. reported that most TSPO-positive glial cells in aged APP tg mouse brains were astrocytes, which expressed glial cell line-derived neurotrophic factor at a high level[14,15], suggesting that TSPO-positive astrocytes may play neuroprotective roles in decelerated amyloid plaque formation and alleviation of abnormal spatial

171

6

learning and memory function. The precise mechanism through which up-regulation of neprilysin activates astrocytes in the brain remains unclear, but neprilysin-generated proteolytic fragments of substrate peptides may be involved in this process.

In conclusion, we have demonstrated that the new gene delivery system based on rAAV9 with a neuron-specific promoter can achieve functional gene expression throughout the brain, but not in peripheral tissues, after intracardiac administration. In our animal model, it could block Aβ accumulation and alleviate cognitive dysfunction based on a water maze test. Furthermore, the expression of neprilysin specifically in endosomes is considered to be advantageous for efficient degradation of Aβ oligomers.

Methods

Recombinant AAV vector production. The AAV vector plasmids contained an expression cassette, consisting of a mouse synapsin I promoter, followed by cDNA encoding neprilysin or its inactive mutant with E585V amino acid substitution, and a woodchuck hepatitis virus post-transcriptional regulatory element between the inverted terminal repeats of the AAV3 genome. The synthesized AAV9 vp cDNA sequence was identical to that previously described[21], except for the substitution of adenine with thymidine at position 1337, which introduced an amino acid change from tyrosine to phenylalanine at position 446[32]. The recombinant AAV vectors were produced by transient transfection of HEK293 cells with the vector plasmid, an AAV3 rep and AAV9 vp expression plasmid, and an adenoviral helper plasmid, pHelper (Agilent Technologies), as described previously[33]. The recombinant viruses were purified by isolation from two sequential continuous CsCl gradients, and the viral titers were determined by qRT-PCR. Before administration, rAAV vectors were diluted in phosphate-buffered saline to $0.5–15 \times 10^{11}$ genome copies/100 μl.

Animals. All animal experiments were approved by the ethics committee at each institute (Nagasaki University, RIKEN Brain Science Institute, National Institute of Radiological Sciences, and Novartis Institutes for Biomedical Research), and performed in compliance with the institutional guidelines. Wild-type and neprilysin-deficient mice (7–9 months old)[10] were randomly assigned to rAAV-SynI::NEP$_{WT}$ vector-injected and rAAV-SynI::NEP$_{MT}$ vector-injected groups. One hundred μl of viral vector solution was injected slowly into circulating blood in the left ventricle of the heart of mice anesthetized with pentobarbital (50 mg/kg, ip) over a period of 1 min with a 0.5 ml syringe equipped with a 29-gauge needle. Male APP transgenic (APP23) mice[11] were randomly assigned to two groups at the age of 17 months, when overt abnormality in learning and memory function was observed in the water maze test. They were housed in plastic cages with food (CE2, Clea Japan, Tokyo, Japan) and water ad lib, and were maintained on a 12/12 h light-dark cycle (lights on at 09:00, off at 21:00).

Immunohistochemistry and quantitative evaluation. One week after amyloid imaging of the vector-injected APP tg mice, the mouse brains were fixed by transcardial perfusion with phosphate-buffered 4% paraformaldehyde and embedded in paraffin. Four-μm-thick sections were mounted onto aminopropyltriethoxysilane-coated glass slides. The brain sections were immunostained using mouse monoclonal anti-neprilysin antibody or mouse monoclonal anti-Aβ antibody against either unmodified amino-terminus of Aβ, N1D, or modified amino-terminus of Aβ, N3pE, and visualized with AlexaFluor 488-conjugated secondary antibody. The sections were observed with a fluorescence microscope, BZ-9000 (Keyence, Osaka, Japan), using a ×2 or a ×4 objective with 1.3× digital zoom, and digital images were captured with a digital microscope camera (Keyence) and saved as digitized tagged-image format files to retain maximum resolution. The density of immunoreactive Aβ deposits in the hippocampal formation and neocortex was measured using image analysis software, MetaMorph, ver. 7.7 (Universal Imaging Corporation, Downington, PA), by an investigator blinded to sample identity. To reduce the variance among tissue sections, we used the average of data from 4 sections per mouse as an individual value.

In addition to Aβ immunolabeling, multiple immunofluorescence staining was performed as described previously[34]. For double staining of neprilysin and cell or organelle marker proteins (NeuN, GFAP, MAP2, tau, syntaxin-1, SV2A, VAMP-1, PSD95, Rab3a, Rab5, Rab7, Rab9, Clathrin, EEA1, Syntaxin-6), brain sections from neprilysin-deficient mice administered with rAAV9-SynI::NEP were first immunostained using a fluorescence-direct TSA method (Texas-Red-conjugated strep-toavidin) combined with anti-neprilysin mouse monoclonal antibody, and then with rabbit polyclonal anti-marker protein antibodies and AlexaFluor 488-conjugated secondary antibody or EnVision plus system HRP-labeled polymer anti-rabbit antibody. The sections were observed under an Axio observer Z1 inverted microscope incorporating a confocal laser scanning system LSM710 with argon, helium/neon (G) and helium/neon (R) lasers (Carl Zeiss Japan, Tokyo, Japan). Alexa 488 and Texas-red were excited with 488 nm and 543 nm laser beams, and observed through 510–530 nm, and 560–600 nm band pass emission filters, respectively. All of the single images were acquired by quintuple scans with ZEN2008, ver. 5.0 software (Carl Zeiss Japan) using a ×63 oil immersion objective, then merged and saved as digitized tagged-image format files to retain maximum resolution.

Behavioral analysis. Five months after the injection of rAAV vector into APP tg mice, the Morris water maze test was conducted as previously reported[5], with minor modifications. Further details are available in the online supplementary information.

In vivo **imaging of amyloid and glial activation.** Positron emission tomographic (PET) scans were conducted for APP tg mice at 20 months of ageas described elsewhere[13,14] with a microPET Focus 220 animal scanner (Siemens Medical Solutions USA, Knoxville, TN) designed for small animals, which provides 95 transaxial slices 0.815 mm (center-to-center) apart, a 19.0-cm transaxial field of view (FOV) and a 7.6-cm axial FOV[35]. Prior to the scans, the mice were anesthetized with 1.5% (v/v) isoflurane. Further details are available in the online supplementary information.

Assay of neprilysin-dependent neutral endopeptidase activity. Hippocampal formations and cerebral cortices were homogenized in five volumes (w/v) of 50 mM Tris-HCl buffer (pH 7.6) containing 150 mM NaCl, protease inhibitor cocktail (EDTA-free Complete™, Roche Diagnostics, Indianapolis, IN) supplemented with 0.7 μg/ml pepstatin A (4397, Peptide Institute, Osaka, Japan) with a Potter-Elvehjem-type grinder (Wheaton, Millville, NJ). The homogenates were centrifuged at 70,000 rpm and 4°C for 29 min using an Optima TL ultracentrifuge and a TLA100.4 rotor (Beckman, Palo Alto, CA). The pellet was solubilized with the above buffer containing 1% Triton X-100 (membrane fraction). NEP-dependent neutral endopeptidase activity in the membrane fraction was fluorometrically assayed using an indirect coupled enzyme assay method. The standard assay mixture consisted of 4–6 μg of membrane fraction, 0.1 mM succinyl-Ala-Ala-Phe-AMC (I-1315; Bachem, Bubendorf, Switzerland) as a substrate, and 100 mM MES buffer (pH 6.5) in a total volume of 50 μL. The reaction was initiated by addition of substrate to the assay mixture, and performed for 1 h at 37°C. To the reaction mixture was then added 2.5 μL of a solution containing 0.1 mg (0.4 units equivalent)/mL leucine aminopeptidase (L-5006; Sigma, St Louis, MO) and 0.2 mM phosphoramidon (4082; Peptide Institute), followed by further incubation for 30 min at 37°C to remove the phenylalanine residue from Phe-AMC generated by neutral endopeptidase-catalyzed digestion. The intensity of the liberated 7-amino-4-methylcoumarin was measured with excitation at 390 nm and emission at 460 nm on a 96-well half-area-black half-well plate using a microplate spectrometer Infinite M-1000 (Tecan Group Ltd., Männedorf, Switzerland). The NEP-dependent neutral endopeptidase activity was determined, based on the decrease in rate of digestion caused by 10 μM thiorphan (T-6031; Sigma), a specific inhibitor of NEP[36]. Protein concentrations were determined using a bicinchoninic acid protein assay kit (Pierce, Rockford, IL).

Aβ quantitation. The cerebral cortices and hippocampi were processed according to the method reported previously[6]. The amounts of Aβx-40 and Aβx-42 in each fraction were determined by sandwich ELISA (Wako, Osaka, Japan).

Western blotting. The Triton X-100-extractable membrane fraction of hippocampi was used for analysing levels of Aβ oligomers and monomers. Protein concentrations were determined using a BCA protein assay kit (Pierce, Rockford, IL). An equivalent amount of protein from hippocampus of each animal was mixed with a 2× sample buffer without a reducing agent, separated by 5–20% gradient SDS-polyacrylamide gel electrophoresis and transferred electrophoretically to a 0.22 μm nitrocellulose membrane (Protoran®, Whatman GmbH, Dassel, Germany). The membrane was boiled in PBS for 3 min to achieve high sensitivity. The blot was probed with anti-rabbit polyclonal antibody against either unmodified amino-terminus of Aβ, N1D (1 μg/ml) or modified amino-terminus of Aβ, N3pE (1 μg/ml)[16], followed by HRP-conjugated anti-rabbit IgG (GE Healthcare, Tokyo). Immunoreactive bands on the membrane were visualized with an enhanced chemiluminescence kit (GE Healthcare), and the band intensities were determined with a densitometer, LAS4000 (Fuji Photo Film, Tokyo, Japan) using Science Lab 97 Image Gauge software (ver. 3.0.1; Fuji Photo Film). Immunoreactive protein content in each sample was calculated based on a standard curve constructed with synthesized Aβ (Peptide Institute, Osaka, Japan). Each set of experiments was repeated at least two times. The blots were reprobed with anti-β-actin (AC-15, Sigma) antibody to confirm that equal amounts of total protein had been extracted.

Statistical analysis. All data were expressed as means ± s.e.m. For comparisons of the means between two groups, statistical analysis was performed by applying Student's *t* test after confirming equality of variances of the groups. If the variances were unequal, Mann-Whitney *U*-test was performed (SigmaPlot software, ver.12.3, Systat Software Inc., San Jose, CA). Comparisons of the means among more than three groups were done by a one-way or two-way analysis of variance (ANOVA) or repeated-measures ANOVA followed by a *post-hoc* test (SigmaPlot software). P values of less than 0.05 were considered to be significant.

Details for antibodies used in this study are available in the online supplementary information.

1. Hardy, J. & Selkoe, D. J. The amyloid hypothesis of Alzheimer's disease: progress and problems on the road to therapeutics. *Science* 297, 353–356 (2002).
2. Iwata, N., Higuchi, M. & Saido, T. C. Metabolism of amyloid-β peptide and Alzheimer's disease. *Pharmacol. Ther.* 108, 129–148 (2005).

172

3. Iwata, N. *et al.* Identification of the major $A\beta_{1-42}$-degrading catabolic pathway in brain parenchyma: suppression leads to biochemical and pathological deposition. *Nat. Med.* **6**, 143–150 (2000).
4. Iwata, N. *et al.* Metabolic regulation of brain $A\beta$ by neprilysin. *Science* **292**, 1550–1552 (2001).
5. Huang, S. M. *et al.* Neprilysin-sensitive synapse-associated amyloid-β peptide oligomers impair neuronal plasticity and cognitive function. *J. Biol. Chem.* **281**, 17941–17951 (2006).
6. Iwata, N. *et al.* Presynaptic localization of neprilysin contributes to efficient clearance of amyloid-β peptide in mouse brain. *J. Neurosci.* **24**, 991–998 (2004).
7. Nilsson, P. *et al.* Gene therapy in Alzheimer's disease - potential for disease modification. *J. Cell. Mol. Med.* **14**, 741–757 (2010).
8. Muramatsu, S. *et al.* A phase I study of aromatic L-amino acid decarboxylase gene therapy for Parkinson's disease. *Mol. Ther.* **18**, 1731–1735 (2010).
9. Christine, C. W. *et al.* Safety and tolerability of putaminal AADC gene therapy for Parkinson disease. *Neurology* **73**, 1662–1669 (2009).
10. Lu, B. *et al.* Neutral endopeptidase modulation of septic shock. *J. Exp. Med.* **181**, 2271–2275 (1995).
11. Sturchler-Pierrat, C. *et al.* Two amyloid precursor protein transgenic mouse models with Alzheimer disease–like pathology. *Proc. Natl. Acad. Sci. USA* **94**, 13287–13292 (1997).
12. Miyakawa, T. *et al.* Neurogranin null mutant mice display performance deficits on spatial learning tasks with anxiety related components. *Hippocampus* **11**, 763–775 (2001).
13. Maeda, J. *et al.* Longitudinal, quantitative assessment of amyloid, neuroinflammation, and anti-amyloid treatment in a living mouse model of Alzheimer's disease enabled by positron emission tomography. *J. Neurosci.* **27**, 10957–10968 (2007).
14. Maeda, J. *et al.* *In vivo* positron emission tomographic imaging of glial responses to amyloid-β and tau pathologies in mouse models of Alzheimer's disease and related disorders. *J. Neurosci.* **31**, 4720–4730 (2011).
15. Ji, B. *et al.* Imaging of peripheral benzodiazepine receptor expression as biomarkers of detrimental versus beneficial glial responses in mouse models of Alzheimer's and other CNS pathologies. *J. Neurosci.* **28**, 12255–12267 (2008).
16. Saido, T. C. *et al.* Dominant and differential deposition of distinct β-amyloid peptide species, $A\beta_{N3(pE)}$, in senile plaques. *Neuron* **14**, 457–466 (1995).
17. Haass, C. & Selkoe, D. J. Soluble protein oligomers in neurodegeneration: lessons from the Alzheimer's amyloid β-peptide. *Nat. Rev. Mol. Cell. Biol.* **8**, 101–112 (2007).
18. Benilova, I., Karran, E. & De Strooper, B. The toxic $A\beta$ oligomer and Alzheimer's disease: an emperor in need of clothes. *Nat. Neurosci.* **15**, 349–357 (2012).
19. Larson, M. E. & Lesné, S. E. Soluble $A\beta$ oligomer production and toxicity. *J. Neurochem.* **120 Suppl 1**, 125–139 (2012).
20. Foust, K. D. *et al.* Intravascular AAV9 preferentially targets neonatal neurons and adult astrocytes. *Nat. Biotechnol.* **27**, 59–65 (2009).
21. Petrs-Silva, H. *et al.* Novel properties of tyrosine-mutant AAV2 vectors in the mouse retina. *Mol. Ther.* **19**, 293–301 (2011).
22. Cirrito, J. R. *et al.* Endocytosis is required for synaptic activity-dependent release of amyloid-β *in vivo*. *Neuron* **58**, 42–51 (2008).
23. Walsh, D. M. *et al.* Naturally secreted oligomers of amyloid β protein potently inhibit hippocampal long-term potentiation *in vivo*. *Nature* **416**, 535–539 (2002).
24. Abramov, E. *et al.* Amyloid-β as a positive endogenous regulator of release probability at hippocampal synapses. *Nat. Neurosci.* **12**, 1567–1576 (2009).
25. Bharadwaj, P. R. *et al.* $A\beta$ aggregation and possible implications in Alzheimer's disease pathogenesis. *J. Cell. Mol. Med.* **13**, 412–421 (2009).
26. Kerr, M. A. & Kenny, A. J. The molecular weight and properties of a neutral metallo-endopeptidase from rabbit kidney brush border. *Biochem. J.* **137**, 489–495 (1974).
27. Selkoe, D. J. Alzheimer's disease is a synaptic failure. *Science* **298**, 789–791 (2002).
28. Holmes, C. *et al.* Long-term effects of Aβ42 immunisation in Alzheimer's disease: follow-up of a randomised, placebo-controlled phase I trial. *Lancet* **372**, 216–223 (2008).
29. Schilling, S. *et al.* On the seeding and oligomerization of pGlu-amyloid peptides (*in vitro*). *Biochemistry* **45**, 12393–12399 (2006).
30. Nussbaum, J. M. *et al.* Prion-like behaviour and tau-dependent cytotoxicity of pyroglutamylated amyloid-β. *Nature* **485**, 651–655 (2012).
31. Schilling, S. *et al.* Glutaminyl cyclase inhibition attenuates pyroglutamate $A\beta$ and Alzheimer's disease-like pathology. *Nat. Med.* **14**, 1106–1111 (2008).
32. Gao, G. *et al.* Clades of adeno-associated viruses are widely disseminated in human tissues. *J. Virol.* **78**, 6381–6388 (2004).
33. Li, X. G. *et al.* Viral-mediated temporally controlled dopamine production in a rat model of Parkinson disease. *Mol. Ther.* **13**, 160–166 (2006).
34. Fukami, S. *et al.* Aβ-degrading endopeptidase, neprilysin, in mouse brain: synaptic and axonal localization inversely correlating with Aβ pathology. *Neurosci. Res.* **43**, 39–56 (2002).
35. Tai, Y. C. *et al.* Performance evaluation of the microPET focus: a third generation microPET scanner dedicated to animal imaging. *J. Nucl. Med.* **46**, 455–463 (2005).
36. Roques, B. P. *et al.* The enkephalinase inhibitor thiorphan shows antinociceptive activity in mice. *Nature* **288**, 286–288 (1980).

Author contributions

S.M. designed and prepared the AAV vectors; N.I. and M. Sekiguchi performed the in vivo experiments, N.I., Y.H., A.T., M.A. performed biochemical and histochemical analyses; B.J. and M.H. performed the PET imaging analysis; M. Staufenbiel provided APP tg mice; N.I., S.M., M.H., M. Staufenbiel and T.C.S. designed the experimental plan and wrote the manuscript.

Additional information

173

Rescue of amyotrophic lateral sclerosis phenotype in a mouse model by intravenous AAV9-*ADAR2* delivery to motor neurons

Takenari Yamashita[1,2,3], Hui Lin Chai[1,2,3], Sayaka Teramoto[1,2,3], Shoji Tsuji[2], Kuniko Shimazaki[4], Shin-ichi Muramatsu[5], Shin Kwak[1,2,3,6]*

Amyotrophic lateral sclerosis (ALS) is the most common adult-onset motor neuron disease, and the lack of effective therapy results in inevitable death within a few years of onset. Failure of GluA2 RNA editing resulting from downregulation of the RNA-editing enzyme adenosine deaminase acting on RNA 2 (ADAR2) occurs in the majority of ALS cases and causes the death of motor neurons via a Ca^{2+}-permeable AMPA receptor-mediated mechanism. Here, we explored the possibility of gene therapy for ALS by upregulating ADAR2 in mouse motor neurons using an adeno-associated virus serotype 9 (AAV9) vector that provides gene delivery to a wide array of central neurons after peripheral administration. A single intravenous injection of AAV9-ADAR2 in conditional ADAR2 knockout mice (AR2), which comprise a mechanistic mouse model of sporadic ALS, caused expression of exogenous ADAR2 in the central neurons and effectively prevented progressive motor dysfunction. Notably, AAV9-ADAR2 rescued the motor neurons of AR2 mice from death by normalizing TDP-43 expression. This AAV9-mediated ADAR2 gene delivery may therefore enable the development of a gene therapy for ALS.

INTRODUCTION

Amyotrophic lateral sclerosis (ALS) is the most common adult-onset motor neuron disease. The lack of an effective therapy for ALS results in death from respiratory muscle weakness within a few years of onset. Therefore, the development of effective therapies is eagerly awaited. However, mechanism-based therapeutic strategies have yet to be developed for this disease. More than 90% of ALS cases are sporadic, and the most of them do not carry mutations in genes that are known to be causative in familial forms of ALS. Rather, loss of TDP-43 from the nucleus with abnormal TDP-43-positive cytoplasmic inclusions (TDP-43 pathology) in motor neurons is the pathological hallmark of sporadic ALS (Aizawa et al, 2010). Furthermore, in the majority of the patients with sporadic ALS, considerable proportions of motor neurons in the spinal cord express abnormal glutamine/arginine (Q/R) site-unedited GluA2 (a subunit of the α-amino-3-hydroxy-5-methylisoxazole-4-propionic acid (AMPA) receptor (Kawahara et al, 2004; Kwak & Kawahara, 2005)) because of reduced expression of an RNA editing enzyme called adenosine deaminase acting on RNA 2 (ADAR2) (Aizawa et al, 2010; Hideyama et al, 2012). Analysis of conditional ADAR2 knockout mice (ADAR2$^{flox/flox}$/VChAT-Cre.Fast or AR2 mice) demonstrated that insufficient ADAR2 expression induced the death of motor neurons via an abnormal Ca^{2+}-permeable AMPA receptor-mediated mechanism (Hideyama et al, 2010). Notably, the expression of abnormal Ca^{2+}-permeable AMPA receptors causes TDP-43 pathology in motor neurons through activation of

(1) CREST, Japan Science and Technology Agency, Graduate School of Medicine, University of Tokyo, Bunkyo-Ku, Tokyo, Japan
(2) Department of Neurology, Graduate School of Medicine, University of Tokyo, Bunkyo-Ku, Tokyo, Japan
(3) Center for Disease Biology and Integrative Medicine, Graduate School of Medicine, The University of Tokyo, Bunkyo-Ku, Tokyo, Japan
(4) Department of Neurosurgery, Jichi Medical University, Shimotsuke, Tochigi, Japan
(5) Department of Neurology, Jichi Medical University, Shimotsuke, Tochigi, Japan
(6) Clinical Research Center for Medicine, International University of Health and Welfare, Ichikawa, Chiba, Japan
*Corresponding author: Tel: +81 3 5841 3566; Fax: +81 3 5841 3566;
E-mail: kwak-tky@umin.ac.jp

calpain, a Ca^{2+}-dependent serine protease, and the resultant expression of aggregation-prone TDP-43 fragments (Yamashita et al, 2012a). The concomitant occurrence of reduced ADAR2 levels and TDP-43 pathology in the same motor neurons (Aizawa et al, 2010) and the presence of calpain-dependent abnormal TDP-43 fragments in the brains and spinal cords of sporadic ALS patients (Yamashita et al, 2012a) suggest that the molecular cascade observed in AR2 mice is similar to what occurs in the motor neurons of ALS patients and that normalization of ADAR2 activity represents a potential therapeutic strategy for ALS patients (Aizawa et al, 2010; Yamashita et al, 2012a, b).

We attempted to broadly deliver ADAR2 cDNA to motor neurons to enhance ADAR2 activity to a level sufficient to edit the Q/R site of GluA2 pre-mRNA. Recently, clinical challenges for gene therapy have been observed when using adeno-associated virus (AAV) as a vector (Lonergan et al, 2005; Mingozzi & High, 2011). Because motor neurons are widely localized in the cranial motor nerve nuclei in the brainstem and the anterior horns of the entire spinal cord, systemic injection of a vector is preferable to local injection to provide global gene delivery to the motor neurons of ALS patients. Although the blood–brain barrier presents a hurdle to the delivery of genes to

the central nervous system from the periphery, several groups have been successful in transducing AAV serotype 9 (AAV9) to foetal, neonatal and adult animal motor neurons in the spinal cord via intravenous administration (Benkhelifa-Ziyyat et al, 2013; Dayton et al, 2012; Duque et al, 2009; Foust et al, 2009). To achieve widespread and selective expression of the *ADAR2* gene in motor neurons and avoid off-target delivery, we used AAV9 as a vector and the synapsin I (SYNI) promoter for neuron-specific expression of ADAR2 cDNA (Supporting Information Fig S1; Iwata et al, 2013).

RESULTS

Examination of ADAR2 activity in cells and mouse brains using AAV9-hADAR2

We constructed cDNA encoding N-terminally Flag-tagged wild-type (WT) human ADAR2a (hADAR2) with the SYNI promoter. After confirming the expression of active hADAR2 protein in Neuro2a cells transduced with AAV9-Flag-hADAR2 (Supporting Information Fig S2; Nishimoto et al, 2008), we confirmed the expression of AAV9-delivered hADAR2 at an effective level
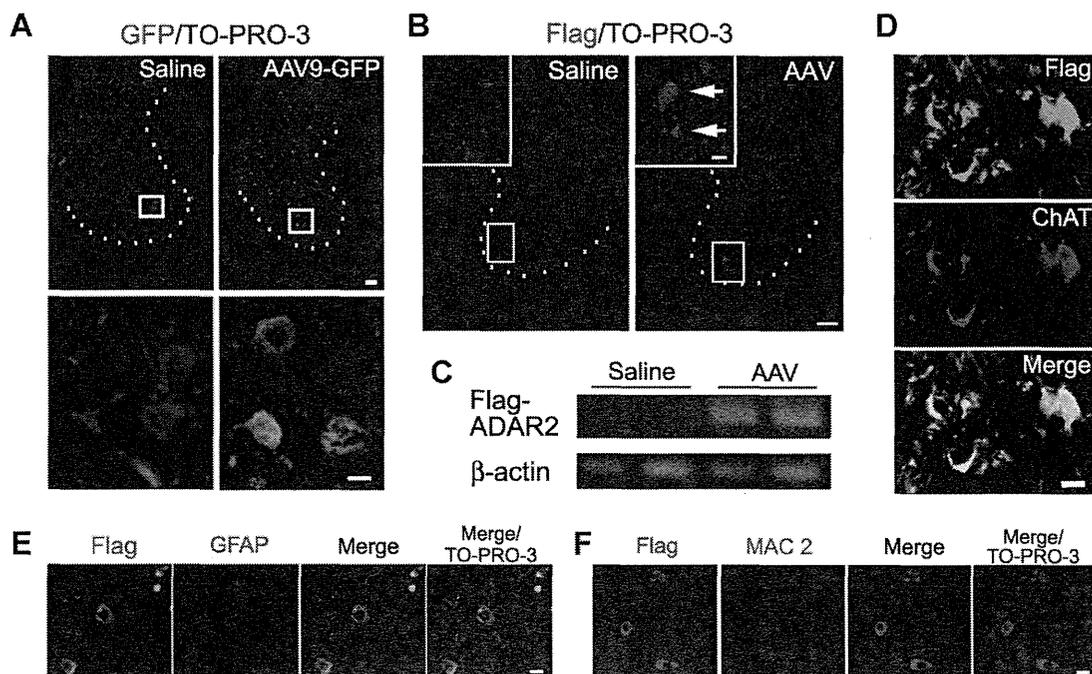
Figure 1. Gene delivery to mouse cortical and spinal neurons using AAV9 vectors.

A. Large motor neurons (anterior horn cells, AHCs) expressed GFP in the spinal cords of wild-type mice injected in the tail vein with AAV9-GFP (1.5×10^{11} vg/body, $n = 4$). Scale bars, 50 μm (upper panels) and 20 μm (lower panels).

B. Expression of Flag protein was observed in the AHCs of AR2 mice injected with AAV9-Flag-hADAR2 in the tail vein (AAV; 2.1×10^{12} vg/body) but not in mice injected with saline (Saline). Arrows indicate Flag-positive AHCs. Scale bars, 50 and 20 μm (insets).

C. RT-PCR demonstrated the expression of Flag-hADAR2 in the anterior horn of AAV9-treated AR2 mice.

D. Representative immunofluorescence images of the spinal cords of AR2 mice treated with AAV9-Flag-hADAR2 showing the expression of Flag (green) and choline acetyltransferase (ChAT) (red) protein using anti-Flag and anti-ChAT antibodies. Magnified view of the boxed areas in Supporting Information Fig S3A. Scale bar, 20 μm.

E. Flag-hADAR2 did not colocalize with GFAP. TO-PRO-3 was used as a cell marker. Scale bar, 20 μm.

F. Flag-hADAR2 did not colocalize with Mac2. TO-PRO-3 was used as a cell marker. Scale bar, 20 μm.

175

in vivo by injecting AAV9-hADAR2^{E396A}, an inactive hADAR2 mutant, directly into the cerebral cortex of WT mice. Because the extensive RNA editing at known ADAR2-specific positions in normal mouse brains (Nishimoto et al, 2008) masked the effects of exogenous ADAR2 expression, we used ADAR2^{E396A} and evaluated the efficacy of gene delivery based on reductions in editing efficiency. The extent of RNA editing at the two ADAR2-specific positions, *i.e.* the Q/R site of the GluA2 pre-mRNA and the K/E site of the cytoplasmic fragile X mental retardation protein interacting protein 2 (CYFIP2) mRNA, was significantly decreased at the site of injection of AAV9-hADAR2^{E396A} but not in the contralateral hemisphere, remote regions (ipsilateral hemisphere 2.0–2.5 mm posterior to the injection site), or brain regions injected with AAV9-GFP (Supporting Information Fig S2D). Delivery of genes packaged in AAV9 into the large anterior horn cells (AHCs) in the mouse spinal cord was confirmed by injection of AAV9-SYNI-GFP (1.5×10^{11} vg/body) into the tail vein of 6-week-old WT mice ($n = 4$/group). Approximately 20% of AHCs were immunoreactive for GFP (Fig 1A).

Gene delivery to cortical and spinal neurons using AAV9 vectors

Consistently, expression of Flag protein and mRNA was demonstrated in the brains and spinal cords (Fig 1B–D and Supporting Information Figs S1 and S3), including the AHCs (Fig 1B and Supporting Information Fig S3B), of AR2 mice injected with AAV9-Flag-hADAR2 in the tail vein (Fig 1B and C). In addition, proliferation of both activated astrocytes showing increased GFAP immunoreactivity and MAC2-positive activated microglial cells was not detected in the spinal cords, including the regions around AAV9-infected neurons of WT mice injected with AAV9-GFP and of AR2 mice injected with AAV9-Flag-hADAR2 (Fig 1E, F and Supporting Information Figs S4 and S5). There was no significant expression of Flag protein in the peripheral organs, as previously reported (Iwata et al, 2013). These results indicate that the intravenously injected AAV9 vector delivers the *ADAR2* gene to neurons and expression of the delivered *ADAR2* in neurons is not toxic without inducing abnormal glial cell reaction.

Behavioural changes in AR2 mice intravenously injected with AAV9-Flag-hADAR2

Next, to test whether a therapeutic level of ADAR2 expression could be achieved through systemic administration, AAV9-SYNI-Flag-hADAR2 was intravenously injected into AR2 mice (2.1×10^{12} vg/body) in the pre-symptomatic stage ($n = 16$; 9–13 weeks old) or after they began exhibiting motor dysfunction to model therapy for patients ($n = 5$; 15 weeks old). Age-adjusted AR2 mice injected with saline were used as controls. AR2 mice provide a mechanistic mouse model of sporadic ALS (Hideyama et al, 2010; Yamashita et al, 2012a). These mice undergo a progressive decline in motor function resulting from the progressive loss of ADAR2-lacking AHCs over a period ranging from 2–3 months to 6–8 months of age (Hideyama et al, 2010); thus, if effective expression of the *ADAR2* gene is achieved by AAV9-hADAR2 infection, motor dysfunction should be ameliorated through the prevention of the death of the AHCs. Mice were observed for behaviour every week until the end point, which was set as the time point at which they failed to stay on the rotarod for more than 10 s or their age exceeded 36 weeks.

Treatment with AAV9-Flag-hADAR2 ameliorated or virtually completely prevented the progressive decline in rotarod performance observed in saline-treated AR2 mice (Fig 2A). This effect on rotarod performance was also evident in AR2 mice treated after the initiation of decline (Supporting Information Fig S6). AAV9-injected AR2 mice exhibited higher spontaneous locomotor activity than saline-injected AR2 mice, but the
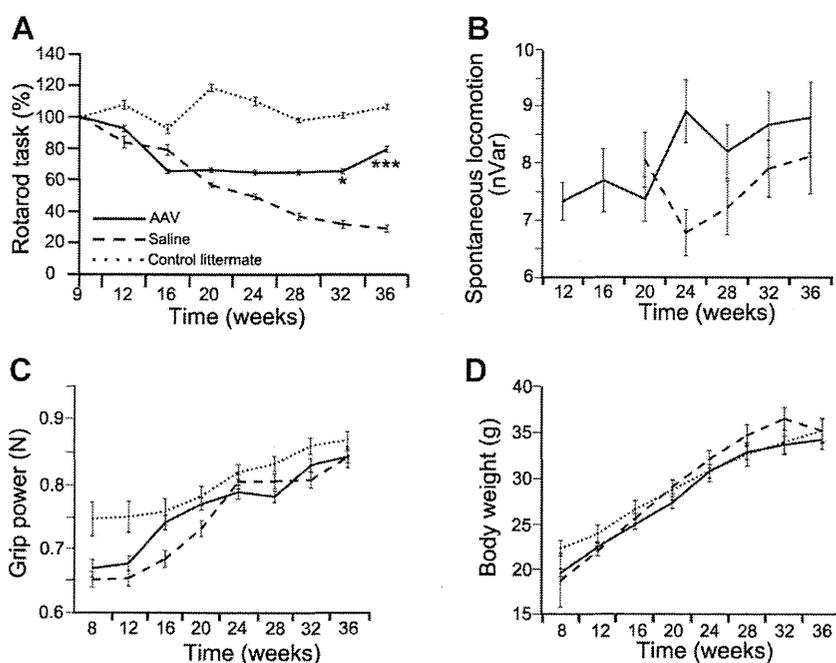
Figure 2. Behavioural changes in AR2 mice intravenously injected with AAV9-Flag-hADAR2.

A. Rotarod performance was significantly better in AR2 mice injected with the AAV9 vector (AAV; $n = 16$) than in saline-treated AR2 mice (Saline; $n = 13$). $^{*}p < 0.05$, $^{***}p < 0.0001$ (Student's *t*-test against Saline). All error bars represent the s.e.m.

B. Spontaneous locomotion was not significantly different between the AAV ($n = 9$) and Saline ($n = 4$) groups. All error bars represent the s.e.m.

C,D. Grip power (C) and body weight (D) did not significantly differ between the AAV ($n = 16$) and Saline ($n = 13$) groups. All error bars represent the s.e.m. Control littermate: Cre-negative, normal littermate mice ($n = 5$). Each plot represents the average value of 4 weeks, and the numbers on the abscissa are the postnatal week indicated as the last week of the 4-week period. Each plot in (A) and (B) represents the value of the latency to fall relative to the value at 9 weeks of age. All error bars represent the s.e.m.

176

difference between the two groups did not reach statistical significance (Fig 2B). The grip power and body weight did not differ between the AAV9-injected and saline-injected AR2 mice (Fig 2C and D). The failure to rescue grip power may be related to the milder motor dysfunction of forelimbs compared to hindlimbs.

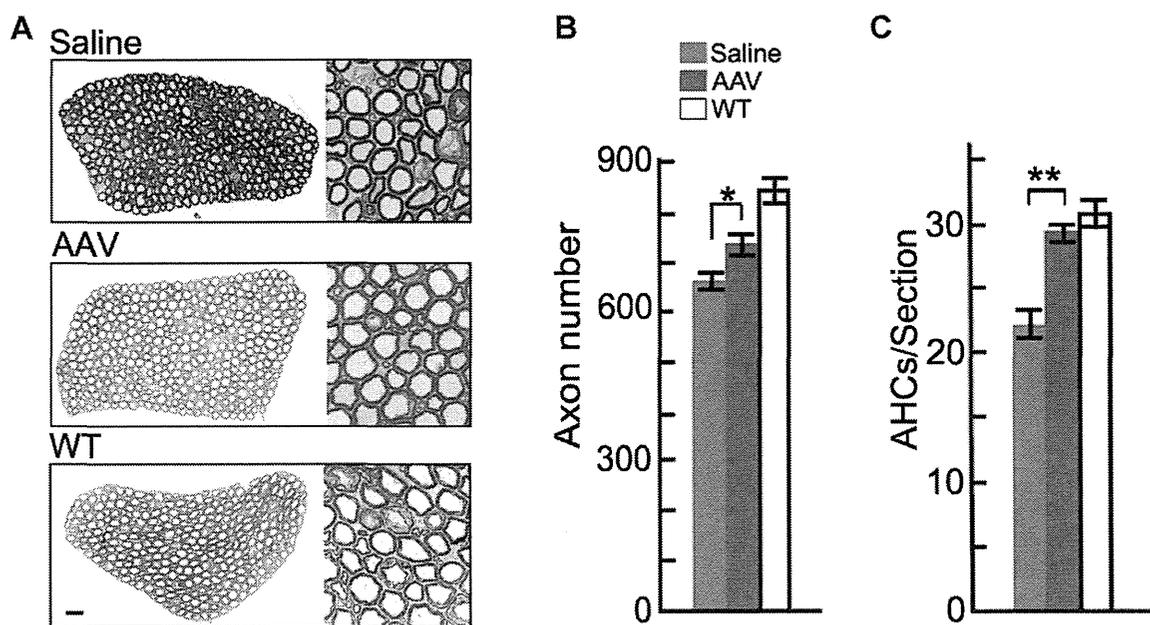### Rescue of motor neurons from death

To confirm that systemic injection of AAV9-hADAR2 prevented the degeneration of AHCs in the AR2 mice, we counted the axons in the ventral root of the fifth lumbar spinal segment (L5) and the number of AHCs in the L5. The number of remaining axons and AHCs was significantly higher in AAV9-injected AR2 mice than in control AR2 mice (Fig 3 and Supporting Information Fig S7). These results indicate that degeneration of AHCs and the resulting motor dysfunction in AR2 mice were effectively prevented by AAV9-mediated delivery of ADAR2.

Rescue of motor neuron functions

Because rescue of death of AHCs likely results from restoration of ADAR2 activity in the motor neurons of AR2 mice (Hideyama et al, 2010), we next investigated whether the expression and activity of ADAR2 were increased in the motor neurons after systemic injection of AAV9-hADAR2. The relative abundance of mouse ADAR2 did not significantly differ between the AAV9-injected and saline-injected AR2 mouse spinal cords (Fig 4A) but

AAV9-Flag-hADAR2 infection induced 1.5-fold increase in the expression level of total ADAR2 mRNA in the spinal cords (Fig 4A) and brains (Supporting Information Fig S8). Messenger RNA of both hADAR2 and choline acetyltransferase (ChAT) was demonstrated in the spinal cord lysates of AAV9-injected AR2 mice (Fig 4B) and the editing efficiency at the GluA2 Q/R site was significantly higher in the remaining motor neurons of AAV9-injected AR2 mice than in those of the control AR2 mice (Fig 4C). These results indicated that hADAR2 was delivered to and functioned in motor neurons. However, ADAR2 protein level did not significantly differ among AAV9-injected AR2 mice, saline-injected AR2 mice and WT mice (Supporting Information Fig S8B and C). The failure to detect the difference despite of the difference in the ADAR2 activity was presumably due to the fact that a modest increase in the ADAR2 expression level with preservation of death of 10–20% of motor neurons in AAV-treated AR2 mice may be masked in ADAR2 expressed in the remaining motor and non-motor neurons and other cells in the anterior horn.

Consistent with the effective prevention of the death of AHCs, loss or mislocalization of TDP-43 in the AHCs of saline-treated AR2 mice was rescued in AAV9-injected AR2 mice, and Flag-expressing AHCs exhibited predominantly nuclear TDP-43 localization (Fig 5 and Supporting Information Fig S9). Indeed, the number of AHCs showing normal nuclear localization of TDP-43 was markedly increased in the AAV9-injected AR2 mice compared with the control AR2


Figure 3. Rescue of motor neurons from death.

A. The ventral root of the fifth lumbar segment (L5). Saline: a saline-injected AR2 mouse, AAV: a pre-symptomatically AAV9-Flag-hADAR2 injected AR2 mouse (AAV), WT: a wild-type mouse (39 weeks of age). Inset; magnified view. Scale bar: 20 and 64 μm for the insets.

B. Numbers of axons in the ventral root in Saline (649.8 ± 17.8, $n = 10$; blue column), AAV (733.0 ± 28.6, $n = 5$; red column), and WT (840.0 ± 26.5, $n = 3$; white column) groups. All error bars represent the s.e.m. *$p < 0.05$ (Student's t-test).

C. Number of AHCs in L5 ($n = 5$ for each group). All error bars represent the s.e.m. **$p < 0.01$ (Student's t-test). Numbers of AHCs in the unilateral AH are presented. Symbol colours are the same as in B.
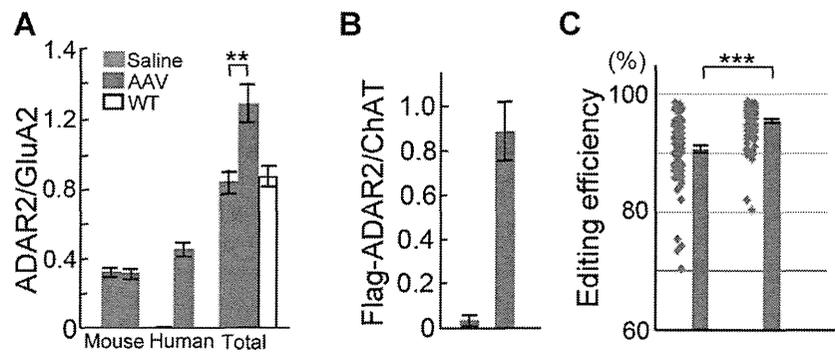
Figure 4. ADAR2 gene expression in the anterior horn of the spinal cord (AH).

A. The relative abundance of mouse ADAR2 mRNA did not significantly differ between AR2 mice injected with AAV9-Flag-hADAR2 (AAV) and those injected with saline (Saline; $n = 5$ for each group). hADAR2 mRNA was expressed at a significant level in AAV. The relative abundance of total (human and mouse) ADAR2 mRNA was 1.5-fold higher in AAV ($n = 4$) than in Saline ($n = 4$). $**p < 0.01$ (Mann–Whitney U-test). All error bars represent the s.e.m.

B. The relative abundance of hADAR2 mRNA standardized with mouse ChAT mRNA indicated that there was significant expression of hADAR2 in ChAT-positive AHCs in AAV. $n = 15$ (AAV) and $n = 6$ (Saline). All error bars represent the s.e.m.

C. The editing efficiency at the GluA2 Q/R site in the AH lysates (four samples from each mouse) from the AAV group ($n = 8$) was significantly higher than that in the control group ($n = 7$) ($95.20 \pm 0.36\%$ vs. $90.68 \pm 0.55\%$; Mann–Whitney U-test, $***p < 0.0001$; ($p = 0.0128$ when compared between AAV and saline groups)). All error bars represent the s.e.m.

mice (Fig 5C and Supporting Information Fig S10). These results indicate that AAV9-mediated delivery of hADAR2 is sufficient to upregulate ADAR2 activity at the GluA2 Q/R site, associated with normalization of TDP-43 pathology in ADAR2-lacking AHCs, thereby preventing neuronal death.

DISCUSSION

In this study, we explored the possibility of using gene therapy to treat ALS by enhancing ADAR2 activity through delivery of the ADAR2 gene to mouse motor neurons using AAV9 as a vector, together with the SYNI promoter to achieve neuron-specific expression of the ADAR2 gene. We showed that AAV9-ADAR2 was successfully delivered to and functioned in motor neurons (Figs 1D and 4 and Supporting Information Fig S3), with a virtual absence of peripheral expression being detected following i.v. administration in the mice. Furthermore, the expression of the delivered ADAR2 prevented the progression of motor dysfunction and neuronal death with restoring ADAR2-mediated RNA editing (Figs 2–4 and Supporting Information Fig S7) without inducing any adverse effects in neurons or surrounding tissues (Fig 1 and Supporting Information Figs S4 and S5) in AR2 mice, which provide a mechanistic model of sporadic ALS (Hideyama et al, 2010; Yamashita et al, 2012a). Notably, effective prevention of the progressive decline in rotarod performance was observed, even after the manifestation of motor dysfunction (Supporting Information Fig S6). Because the death of ADAR2-deficient AHCs is prevented by the expression of Q/R site-edited GluA2 in the absence of ADAR2 in homozygous and heterozygous AR2 mice (Hideyama & Kwak, 2011; Hideyama et al, 2010, 2012), our results indicate that AAV9-mediated delivery of hADAR2 enables the restoration of ADAR2 activity in ADAR2-deficient AHCs to a level that is sufficient to edit the Q/R

sites of virtually all of the GluA2 pre-mRNAs expressed in AR2 mice (Fig 4 and Supporting Information Fig S8). Given that the level of ADAR2 reduction is more modest in the motor neurons of patients with sporadic ALS (Hideyama et al, 2012; Kawahara et al, 2004) compared to the AHCs of AR2 mice in which ADAR2 is absent (Hideyama et al, 2010), a therapeutic level of ADAR2 activity would be more easily achieved in ALS patients using this method of gene delivery.

In the AAV9-treated AR2 mice, TDP-43 immunoreactivity was observed to be predominantly nuclear in Flag-positive AHCs, as in normal mouse AHCs, which is in marked contrast to the absence of TDP-43 immunoreactivity or the presence of numerous cytoplasmic TDP-43 immunoreactive aggregates found in ADAR2-lacking AHCs from untreated AR2 mice (Fig 5 and Supporting Information Fig S9). TDP-43 pathology in motor neurons of the spinal cord is the pathological hallmark of ALS (Aizawa et al, 2010; Arai et al, 2006; Neumann et al, 2006), and mislocalization of TDP-43 is induced by exaggerated calpain-mediated cleavage of TDP-43 into aggregation-prone fragments, although further activation of calpain cleaves the aggregation-prone fragments into smaller soluble fragments (Yamashita et al, 2012a). The abnormal activation of calpain is a consequence of an increased Ca^{2+} influx through Ca^{2+}-permeable AMPA receptors containing Q/R site-unedited GluA2 in the ADAR2-deficient AHCs of AR2 mice, and expression of edited GluA2, even in the absence of ADAR2, rescues TDP-43 mislocalization and AHC loss by normalizing calpain activity (Yamashita et al, 2012a). Therefore, it is likely that ADAR2 delivery normalized the subcellular localization of TDP-43 in the AHCs by reducing Ca^{2+} influx through AMPA receptors and the resulting calpain activation. Our results demonstrating the AAV9-ADAR2-mediated normalization of TDP-43 provide additional evidence that ADAR2 deficiency represents a cause of ALS.

178
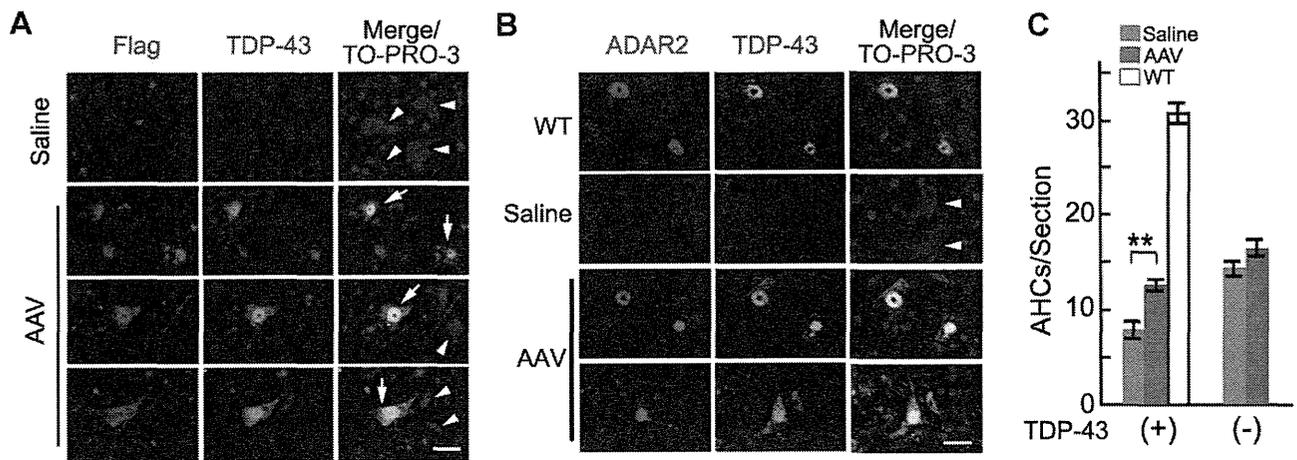
Figure 5. Rescue of TDP-43 in motor neurons.

A. Immunohistochemistry for TDP-43 (green) and Flag (red) in the spinal cord. AHCs were recognized as large ($\geq$20 μm diameter) and TO-PRO-3-positive (blue) cells in the AH. Flag-positive AHCs exhibited intense nuclear and faint cytoplasmic TDP-43 immunoreactivity (arrows) in AAV9-injected AR2 mice (AAV). Arrowheads indicate AHCs negative for both Flag immunoreactivity and TDP-43 immunoreactivity in the nucleus in saline-injected AR2 mice (Saline) and AAV. TO-PRO-3 was used as a cell marker. Scale bar is 20 μm.

B. Double immunostaining of the AH for TDP-43 and ADAR2. The nuclei of the AHCs were either double-positive or double-negative for TDP-43 (green) and ADAR2 (red) in AAV, Saline and wild-type mice (WT). Scale bar is 20 μm.

C. Number of TDP-43-positive and -negative AHCs in Saline (blue columns), AAV (red columns) and WT (white column) ($n = 5$ for each group). All error bars represent the s.e.m. $**p < 0.01$ (Student's t-test).

Delivery and expression of target genes has been achieved using AAV9 with the cytomegalovirus (CMV) or CMV enhancer/beta-actin (CB) promoter in many cell types including neurons (Benkhelifa-Ziyyat et al, 2013; Thevenot et al, 2012), but off-target overexpression of genes may have deleterious effects. Here, using our neuron-specific AAV9-SYNI vector, we were successful in limiting target gene expression to neurons with a virtual absence of expression in peripheral tissues. Recent reports in human patients have shown that the effects of gene delivery by direct injection of AAV2 vectors into the brain continue for up to 12 months without serious adverse effects (Hwu et al, 2012), and we found strong and long-term expression of *ADAR2* in mouse motor neurons. The ADAR2 transgenic mice were phenotypically normal except for moderate obesity (Singh et al, 2007), which suggests that expression of the exogenous ADAR2 gene is relatively safe.

Taken together, our results indicate that therapy through replacement of deficient ADAR2 protein is a logical approach to therapeutic intervention for ALS that could be effective in the majority of ALS patients and that given the demonstrated effects and safety of the clinical use of AAV, gene therapy using AAV9-hADAR2 is a promising therapeutic strategy for ALS. The appropriate route of administration and the required dose of AAV should be determined in future studies. The results from our ALS model mice and recently reported results from Alzheimer's disease model mice (Iwata et al, 2013) suggest that AAV vector-mediated cDNA delivery to central neurons through the vasculature using neuron-specific promoters as regulators of gene expression is a new therapeutic approach for the treatment of neurodegenerative diseases.

MATERIALS AND METHODS

Antibodies

The primary antibodies were as follows: rabbit anti-human beta-actin (IMGENEX Corp.); goat anti-ADAR2 (E-20) (Santa Cruz Biotech.); rabbit anti-GFP (Cell Signaling Technology, Danvers); rabbit anti-DYKDDDDK tag (Flag) (Cell Signaling Technology); goat anti-DDDDK tag (Abcam); sheep anti-rat RED1 (ADAR2, Exalpha Biologicals, Inc.); rabbit anti-glial fibrillary acidic protein (GFAP) (Lab Vision); rat anti-mouse MAC-2 (Cedarlane); goat anti-choline acetyltransferase (ChAT) (Millipore); and rabbit anti-human TDP-43 (10782-1-AP, ProteinTech Group, Inc., designated as TDP-43).

The secondary antibodies used for immunohistochemistry were as follows: Alexa Fluor 488 goat anti-rat IgG; Alexa Fluor 488 chicken anti-rabbit IgG; Alexa Fluor 555 donkey anti-goat IgG; Alexa Fluor 555 goat anti-rabbit IgG; Alexa Fluor 555 goat anti-rat IgG; Alexa Fluor 555 donkey anti-sheep IgG (Invitrogen); and the HRP-DAB System (Vector Co.). Peroxidase-conjugated goat anti-rabbit IgG and peroxidase-conjugated horse anti-mouse IgG (Cell Signaling Technology, Inc., Danvers) were used for immunoblot analyses.

Reagents

TO-PRO-3 was purchased from Invitrogen.

Construction of plasmids

To generate full-length human ADAR2 expression constructs, we first amplified the coding region from human ADAR2a cDNA (hADAR2) generated from the human HeLa cell line using the primers ADAR2UP1 (5'-AAAAAGAATTCATGGATATAGAAGATGAAGAAAC-3') and ADAR2DW1 (5'-AAAAATCTAGATCAGGGCGTGAGTGAGAACTGGTCC-3'). After gel purification, the PCR products were digested with *EcoRI* and *XbaI* and

179